Research Square

Preprints are preliminary reports that have not undergone peer review.
They should not be considered conclusive, used to inform clinical practice,
or referenced by the media as validated information.

Global extreme wave estimates and their sensitivity to the analysed data period and data sources

Khalid AMAROUCHE (khalidamarouche@uludag.edu.tr)
Uludağ University
Adem AKPINAR
Uludağ University
Bahareh KAMRANZAD
Imperial College London
Ghollame-Ellah-Yacine KHAMES
University Yahia Fares of Medea

Research Article

Keywords: Global extreme waves, Annual maximum, Peak-over-threshold, extreme value analysis, Generalized extreme value distribution, Generalized Pareto distribution

Posted Date: September 22nd, 2022

DOI: https://doi.org/10.21203/rs.3.rs-2069865/v1

License: This work is licensed under a Creative Commons Attribution 4.0 International License.
Read Full License

Additional Declarations: No competing interests reported.

Global extreme wave estimates and their sensitivity to the analysed data period and data sources

Khalid AMAROUCHE[1,*]., Adem AKPINAR[1]., Bahareh KAMRANZAD [2,3,4] and Ghollame-Ellah-Yacine KHAMES [5]

[1] Bursa Uludağ University, Department of Civil Engineering, 16059, Bursa, Turkey

[2] Kyoto University, Hakubi Center for Advanced Research, Kyoto, 606-8501, Japan

[3] Kyoto University, Graduate School of Advanced Integrated Studies in Human Survivability (GSAIS), Kyoto, 606-8306, Japan

[4] Department of Physics, Faculty of Natural Sciences, Imperial College London, London SW7 2AZ United Kingdom

[5] Yahia Fares University of Medea Department Natural Sciences, Médéa, Algeria

Abstract

In the lack of wave measuring buoys operating over extended periods, the use of wave hindcast data or satellite observations is indispensable for estimating global extreme wave heights. However, the results may depend on the analysed wind wave sources and the length of the analysed period. The sensitivity of the estimated extreme significant wave heights (SWH) to the analysed data sources and periods is investigated in this study. Global extreme wave heights are estimated using ECMWF Reanalysis v5 data (ERA5), global wave hindcast developed based on Simulating WAves Nearshore forced by the Japanese 55-year Reanalysis (SWAN-JRA55), satellite altimeter observations, and long-term wave buoy measurements. Both Annual Maximum fitting to the Generalized Extreme Value Distribution (AM-GEV) and Peaks Over Threshold fitted to the Generalized Pareto Distribution (POT-GPD) models are used. The results show that the global extreme SWH estimates considerably depend on the analysed data sources. The relative differences observed between the analysed data sources are >20% in large part of the world. Thus, by increasing the analysed data periods, the relative differences in extreme SWH are mainly lower, but they can reach 30% and are more important using AM-GEV. Besides, by comparing the extreme values from reanalysis and hindcast wave data to those from long-term wave measurements, underestimations of up to 2 m are observed for a return period of 100 years in the North-West Atlantic and North-East Pacific.

Keywords: Global extreme waves; Annual maximum; Peak-over-threshold; extreme value analysis; Generalized extreme value distribution; Generalized Pareto distribution

*: Corresponding author: Khalid Amarouche, Tel.: +90 553 959 8211.
E-mail: khalidamarouche@uludag.edu.tr , amarouchekhalid@gmail.com , Address: Uludağ Üniversitesi İnşaat Mühendisliği Bölümü, Görükle Kampüs-Nilüfer, 16059, Turquie.
orcid.org/0000-0001-7983-4611.1

1. Introduction

Estimating the extreme waves for specific return periods is among the most essential and critical information required for various coastal and offshore engineering applications (Campos et al. 2019), such as the design of offshore and coastal structures (Panchang et al. 2013) and naval architecture (Buxton and Stephenson 2001; Caires et al. 2006). A reliable estimation of the extreme significant wave height (SWH) is crucial to secure, sustainable, and economical designs in all marine facilities. The accurate estimate of the extreme wave climate may depend on several factors, e.g., the accuracy of the used wave hindcast data or wave observation (Wada and Waseda 2018, 2020), the size of the analysed sample (Orimolade et al. 2016), and the considered period (Cai and Hames 2010). Thus, as demonstrated by several researchers, the estimated extreme wave conditions depend on the methodology used for the extreme value analysis (EVA) (Sartini et al. 2015b; Orimolade et al. 2016; Samayam et al. 2017). The climate change phenomena may also affect the estimated values of the extreme SWH (Grabemann et al. 2008; Lobeto et al. 2021; Vieira et al. 2021). The most widely used statistical models are the annual maximums fitted to the generalized extreme value distribution (AM-GEV model) and the peak over the thresholds fitted to the generalized Pareto distribution (POT-GPD model). The accuracy of these statistical models depends mainly on the goodness of fit between the theoretical distribution and the analysed data and on the confidence interval of the estimated distribution parameter (Soukissian and Tsalis 2015).

The wave climate distribution may change depending on the time period and data availability. The inter-annual variability in wave climates can lead to variations in the SWH distribution parameters and, therefore, in the results of extreme value analyses. On the other hand, from a statistical point of view, large sample size may reduce the confidence intervals. However, the shape of the distribution may also change depending on the sample size, which may change the goodness of the fit against the used distributions. Hence, the present study aims to evaluate the sensitivity of the global extreme SWH estimates to the data sample sources and characteristics, size or time period, and the used models. As we noticed through the results of the estimated global extreme SWH in the previous studies, the results can be widely distinct in several regions. These studies (Alves and Young 2003; Mori et al. 2010; Vinoth and Young 2011; Yang and Oh 2018; Takbash and Young 2019, 2020) used different data sources, analysed periods, and methods. The sensibility to the used model was previously evaluated by (Soukissian and Kalantzi 2006; Sartini et al., 2015b; Orimolade et al. 2016). Thus, Cai and Hames (2010) and Orimolade et al. (2016) evaluate the uncertainty related to the sample size in the Barent Sea. In

68 the present study, the extreme wave analysis was applied using two models, i.e., POT-GPD and
69 AM-GEV, and with four different wave data sources; i) a 60-year wave hindcast dataset
70 developed using the Simulating Wave Nearshore (SWAN) (Booij et al. 1999; Ris et al. 1999)
71 model forced by Japanese 55-year Reanalysis (JRA-55) wind reanalyses, ii) the fifth generation
72 ECMWF wave reanalyses (ERA5) for 40 years, iii) the satellite observations calibrated and
73 provided by IFREMER for 20 years, and iv) wave buoy measurements provided by Copernicus
74 at 40- and 30-year periods. In all analyses, the maximum likelihood estimators (MLE) are
75 considered for estimating distribution parameters. This method was recommended by
76 Mathiesen et al. (1994) and has been widely used since then (Coles 2001; Caires et al. 2006;
77 Mazas and Hamm 2011; Neary et al. 2020). However, the sensitivity of the results to the used
78 parameters estimate method was not evaluated in the present study. For the evaluation of the
79 goodness of fit in both used distributions (GEV and GPD), it was assessed using the
80 Kolmogorov-Smirnov test (K-S test), advised by Mathiesen et al. (1994), and applied
81 independently for each location in the globe, for all analysed data sources and for the different
82 periods considered. The K-S test was used in several studies (Mínguez et al. 2013; Agarwal et
83 al. 2013), focusing on estimating the extreme SWH.

84 The particularity in the present study consists of evaluating both sensitivities of the wave
85 distribution and estimated extreme waves to both sample size and data sources on a global scale.
86 Thus, a new approach for threshold selection on a global scale was proposed to ensure a reliable
87 comparison of extreme SWH estimates of different datasets. Noting that the selected threshold
88 depends on the wave climate at the chosen location, the wave climate of the analysed period
89 and data sources are independently considered. The proposed method for selecting the threshold
90 at a global scale is derived from the one proposed by Bernardara *et al.* (2014) and consists of
91 defining the threshold value for which the exceeding independent data best fits the GPD. The
92 best fit in the present study is defined based on the K-S test. Knowledge of the sensitivity of
93 extreme wave estimates to sample size and data sources can be very valuable for engineering
94 applications and decision-makers. It can be important to determine the minimum duration and
95 good data sources to be considered for a more accurate estimation of extreme SWHs depending
96 on the study region, as well as to appreciate the probable uncertainties in the estimated extreme
97 wave analysis results.

98

99

2. Methodology

The extreme wave analysis is mainly performed using theoretical distribution functions (Goda 2000). The observed wave data can be statistically fitted to different distribution functions. The distribution of the retrospective wave climate data determines the privileged distribution. The selected distribution functions can be assessed by a goodness of fit test. However, there is no theoretical evidence to establish a standardized distribution model (Mathiesen et al. 1994). Currently, one of the most used and recommended distribution models for extreme wave height analysis is the POT-GPD, which according to Cañellas et al. (2007), provides a proper estimation for wave climate analysis. The AM-GEV model is also recommended and widely used (Cañellas et al. 2007; Sartini et al. 2015a; Saeed Far and Abd. Wahab 2016; Sulis et al. 2017). However, long-term wave data are required for using this model.

A simple and reproducible approach is applied to assess the sensitivity of the extreme wave estimated results to the used methods, the analysis data period, and the used data sources. Those data include wave buoy measurements, satellite observations, wave reanalysis, and modeled wave hindcast. We divided the data in time by ten years scale factor for the last three wave data sources. The shape parameters are estimated for each dataset using the MLE method, and the goodness of fit of the different used data sets against two used distribution models was tested using K-S test. The K-S test results concerning the data with significant fit were mapped. On the other hand, for each analysed dataset, the upper confidence interval of the estimated shape and scale parameters are computed for a confidence level of 95% and mapped. Based on the estimated distribution parameters of each dataset, the returned period results obtained for different data sources and different data periods using AM-GEV and POT-GEV distribution models were estimated, inspected, and compared through global spatial maps. The extreme waves for a return period up to 100 years are also estimated using offshore buoy measurements and compared graphically to those obtained from the ERA5 reanalysis data and JRA-55 wave hindcast data at the nearest location. Thus, the goodness of fit of each data set against both distribution models (GEV and GPD) was evaluated using K-S test, considering a confidence level of 95% for a significant fit.

As there is no theoretical approach to validate the estimated extreme wave values, we consider that the more probably correct estimations are the results obtained using the buoy measurement data set, with a more considerable analysed period and a proper fit to the used distribution model.

2.1. AM-GEV model

One of the most used techniques for investigating extreme waves for different return periods is the AM-GEV model. This approach involves using the GEV cumulative distribution and adjusting the yearly maxima values. The Gumbel, Frechet, and Weibull families of distributions are assembled as GEV Distribution family. Following is a description of the GEV's cumulative distribution function:

$$G(x) = \exp\left\{-\left[1 + \xi\left(\frac{x-\mu}{\sigma}\right)\right]^{-1/\xi}\right\} \quad (1)$$

The three parameters of the GEV distribution are the shape parameter ξ ($-\infty < \xi < \infty$), scale parameter σ ($\sigma > 0$), and location parameter μ. The Gumbel family corresponds to Type I of the tail if ξ equals zero; the distribution function in this situation is explained as follows:

$$G(x) = \exp\left\{-\exp\left[-\left(\frac{x-\mu}{\sigma}\right)\right]\right\} \quad (2)$$

When ξ is less than zero, it is referred to as having a tail Type II (Frechet distribution family). When ξ is greater than zero, it is admitted that the GEV has a tail of Type III that matches the Weibull distribution family. To estimate these GEV distribution parameters, MLE is used. The following equation describes the estimation of the likely return values Z_m over a return period of m years based on the AM-GEV approach.

$$Z_m = \begin{cases} \mu - \frac{\sigma}{\xi}\left[1 - \left\{-log\left(1 - \frac{1}{m}\right)\right\}^{-\xi}\right], & if\ \xi \neq 0 \\ \mu - \sigma \ln\left[-log\left(1 - \frac{1}{m}\right)\right], & if\ \xi = 0 \end{cases} \quad (3)$$

Utilizing AM-GEV method allows us to analyze the same amount of data, the same simple size at the same duration, and a more objective comparison between the different return levels obtained using different data sources.

2.2. POT-GPD model

Using the POT-GPD for estimating the return periods of extreme waves, we consider the series of values x_i, ...x_n from 'n' independent SWH values. After a specific threshold value (u) is defined, the values exceeding the amount of u are filtered and then adjusted to the GPD. The

158 shape parameter ξ (−∞ < ξ < ∞) and the scale parameter σ (σ > 0) are the two parameters of
159 GPD, and the distribution function is given by

$$F(y) = \begin{cases} 1 - \left(1 + \xi \frac{y}{\sigma}\right)^{\frac{-1}{\xi}} & if\ \xi \neq 0 \\ 1 - exp\left(-\frac{y}{\sigma}\right) & if\ \xi = 0 \end{cases} \quad (4)$$

161 When ξ=0, the GPD is expected to have a tail of Type I (exponential distribution). Otherwise,
162 it is assumed that the GPD has a tail Type II similar to the Pareto distribution if ξ>0. If ξ< 0,
163 the tail is Type III, a case of the beta distribution.

164 The maximum value of x that is expected to return at least once within the next m years can be
165 found by solving the following function using the POT-GPD approach to estimate the likely
166 return values during a return time of m.

$$f(x_m) = \zeta_U \left[1 + \xi \left(\frac{x_m - u}{\sigma}\right)\right]^{-1/\xi} = \frac{1}{m} \quad (5)$$

168 where f(x) is the GPD's probability density function, ζ_U is the probability that the value of x
169 exceeds the threshold value u (ζ_U = Pr{ X > u}) (Saeed Far and Abd. Wahab 2016), and the
170 equation that follows is a solution to determine the return level, x_m:

$$x_m = \begin{cases} u + \frac{y}{\sigma}\left[(m\,\zeta_u)^{\xi} - 1\right], & if\ \xi \neq 0 \\ u + \sigma\, log(m\,\zeta_u), & if\ \xi = 0 \end{cases} \quad (6)$$

172 where m is the average number of events during a return period. According to (Goda 2010), the
173 POT approach allows for an increase in mean rate and sample size, which reduces the return
174 value's standard deviation.

175

176 **2.3.Threshold selection**

177 Setting the threshold is a tricky challenge in POT approach. The threshold value selection must
178 be based on the meteorological data in the study area, as advised by Mathiesen et al. (1994). To
179 achieve a robust fit, it is important that the threshold selected for the POT-GPD model is set
180 high enough and that a sufficient number of peaks are identified. For the choice of adequate
181 threshold values, several methods are applied. Coles (2001) presented graphical approaches to
182 select an appropriate threshold, which consists of observing the stability of the Pareto shape
183 parameters (ξ) and the modified scale ($\sigma^* = \sigma_u - \xi_u$) or the mean residual life plot concerning the
184 dataset that exceeds different threshold values. The estimated parameters are plotted as a

function of their corresponding threshold, and finally, the appropriate threshold is defined graphically based on the plot stability (see Coles 2001). The estimated parameters are nearly constant for the given u threshold values before becoming very variable due to the smaller sample size (Caires 2016). The accuracy of this method is subjective and may be affected by observer error, and may not be appropriate on a global scale and for an accurate comparison between results obtained by employing the same model with different data sources and different data lengths. Limiting the subjectivity associated with the graphical threshold selection is necessary to guarantee that outcomes from various points are similar and repeatable (Nicolae Lerma et al. 2015). Thus, a minimum time interval between two successive peaks should be defined to ensure that the fitted datasets are independent peaks. Mathiesen *et al.* (1994) have recommended a minimum local maximum of 2 days. The present study uses a minimum of 2 days' peak interval.

As the graphical method is not automatic and practically unfeasible manually on a global scale, and as there is no theoretical approach for the threshold selection, we applied a complex but programmable method for threshold estimations. This method selects the threshold for which the exceeding data that significantly fit GPD shows the highest confidence level using the K-S test. The goodness of fit for the datasets exceeding all evaluated threshold values is tested using K-S test and compared based on the obtained significant confidence level values. If the confidence levels are similar for different tested threshold values, the lowest threshold is considered to increase the data sample size. For this purpose, an iterative approach was used. The threshold selection was performed separately for each evaluated data source and location. Thus, the peaks are filtered by considering the maximum peak value from the non-independent storms. The used approach allows an automatic and objective selection of the threshold on a global scale by ensuring that the data over the threshold significantly fit the GPD with the highest confidence level. This approach deviates from that proposed by Bernardara *et al.*, (2014) and is adapted for a global spatial application on multiple sources. The approaches proposed by Bernardara *et al.* (2014) is based on two complementary steps: the first is to ensure a sample of independent values, and the second is to fix the optimal convergence threshold towards the GPD. In the previous study, the 70^{th} percentile was defined as a minimum recommended threshold for North Pacific regions (Takbash and Young 2020). Thus, a fixed threshold percentile of 90^{th} and 95^{th} was also globally used in literature (Takbash and Young, 2019; Gramcianinov et al. 2020). The threshold values selected in this study are shown in Figure 1. The selected thresholds vary depending on the analysed dataset. The threshold values increase slightly with the increasing sample period. The threshold values obtained from the

satellite observation are much lower than those selected for ERA5 and SWAN-JRA-55. The thresholds varied between 2 m and 3 m in the equatorial regions and reached 8-10 m in the Southern Ocean and the northern Pacific using SWAN-JRA-55 and ERA5 datasets. For satellite observations, the maximum threshold is 6 m in the North Atlantic and reaches 7 m in the Southern Ocean.

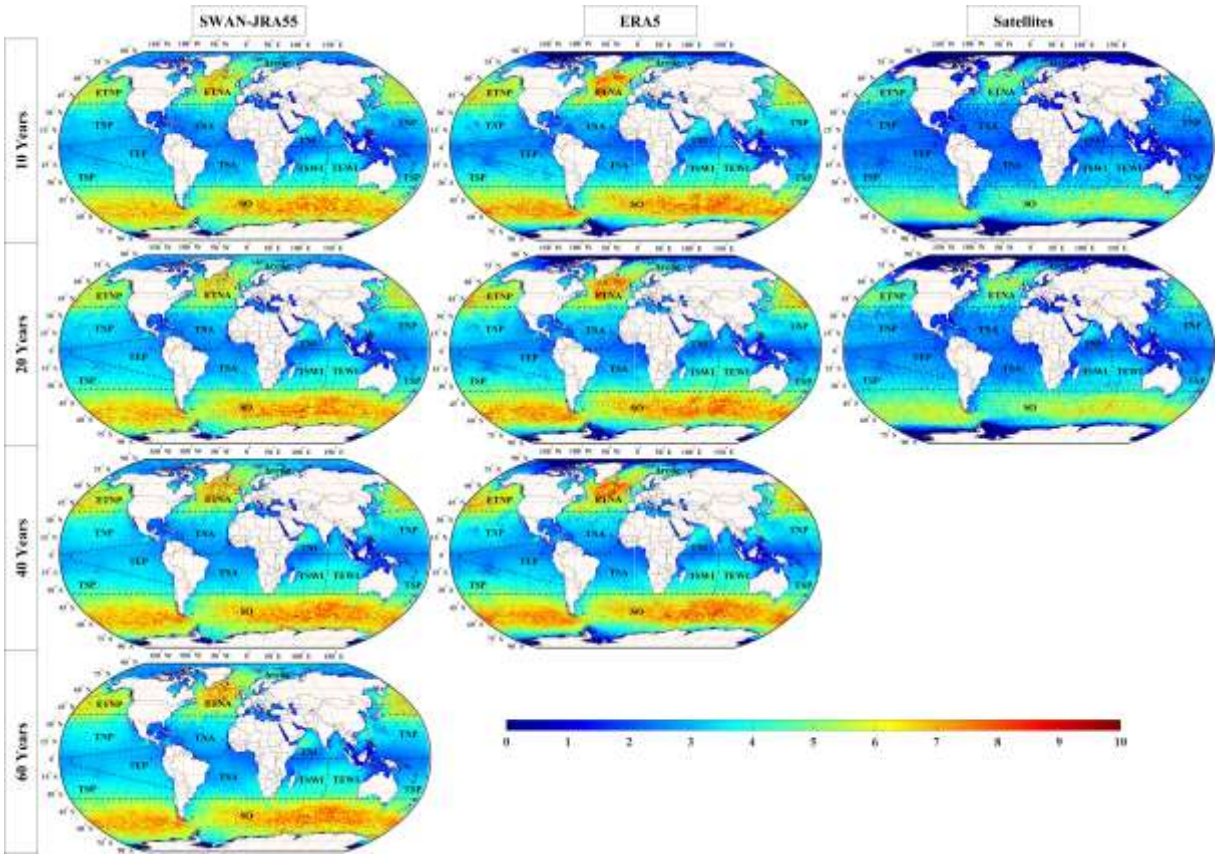


Figure 1. Threshold values providing a significant fit to GPD distribution, with the highest p-value estimated based on K-S test

2.4. Distribution parameter estimator

To define the theoretical distribution shape for the analysed data, the distribution parameter should be estimated. For this, several estimate methods can be used, e.g., the graphical fitting method, the least squares method, the method of moments, and the maximum likelihood method. Those methods were evaluated by Van Vledder *et al.*, (1994), who estimated the extreme SWH for a 100-year return period using different distribution parameter estimation methods for both POT-GPD and AM-GEV models and found slight differences comparing the estimated results. They found that using POT-GPD showed more differences related to the selected threshold u (Van Vledder et al. 1994). In the present study, the MLE is used for

estimating the GPD parameters for POT-GPD model and for estimating the GEV distribution parameters for AM-GPD model. The MLE method is carefully analysed and explained in (Fisher 1925; Wilks 1938; Kendall and Alan 1961). According to Mathiesen et al. (1994), the MLE is considered to be suitable for extreme wave analysis.

Using an iterative numerical scheme, The MLE determines by iteration the distribution parameters that maximize the likelihood function.

$$L(x_1 \dots \dots \dots x_n;\ a_1 \dots \dots \dots a_m) = \prod_{m=1}^{N} f(x_i;\ a_1 \dots \dots \dots a_m) \quad (7)$$

where x_i is the observed data values, and f() is the probability density function maximized by the parameters a_i (Mathiesen et al. 1994; Goda 2010). In the presented study, MATLAB R2021b MLE function was used.

2.5. Goodness of fit test

Statistical methods based on EVA have shown promising results in predicting these events in several scientific fields (Thomas et al., 2016; Butturi-Gomes et al. 2019). Evaluating the goodness of fit of probabilistic models is a very important task in analyzing extreme events. This step is consolidated by using goodness-of-fit tests such as Kolmogorov-Smirnov, which is widely used (Yuan et al. 2018; Martins et al. 2020; Elgohari and Yousof 2021). The K-S test was used to compare the theoretical and empirical cumulative distributions (Wilks 2011).

The Kolmogorov-Smirnov goodness-of-fit test, also called the Kolmogorov-Smirnov one-sample test, examines how well an observed cumulative frequency distribution conforms to an expected frequency distribution (Zar 2013). The Kolmogorov–Smirnov goodness-of-fit test is used in many applications in climate research. Kolmogorov Statistics is recommended for tests of fit for the Extreme Value and Weibull Distributions (Chandra et al. 1981). In the K-S test, the null hypothesis (H_0) is defined as the data fit a specified distribution. In contrast, the alternative hypothesis (H_1) is that the data do not fit the specified distribution utilizing the one-sample Kolmogorov-Smirnov test in Matlab 2021b. At a 5% significance level, the test rejects the null hypothesis. The K-S test statistic is defined as:

$$D = max_{1 \le i \le N} \left(F(Y_i) - \frac{i-1}{N}, \frac{i}{N} - F(Y_i) \right) \quad (8)$$

where F is the theoretical cumulative distribution of the distribution being tested which must be a continuous distribution (i.e., no discrete distributions such as the binomial or Poisson), and

it must be fully specified (i.e., the location, scale, and shape parameters cannot be estimated from the data). The hypothesis regarding the distributional form is rejected if the test statistic, D, is greater than the critical value.

3. Wave data

3.1. Buoy measurements

For a robust extreme wave estimate and to assess the sensitivity of the estimated results to the used wave data source's accuracy, wave buoy measurements over a long period of 30 years and 40 years were used for extreme wave estimate. The extreme values estimated for return periods between 2 and 100 years are compared graphically to those estimated using hindcast wave data and reanalysis wave data at the buoy's locations. The wave buoy measurements used in this study are provided by the Copernicus Marine Environment Monitoring Service (CMEMS) https://marine.copernicus.eu/ (last accessed 16.11.2020), and only offshore buoys were considered. The offshore buoys providing a non-interruptible measurements dataset with a low number of missing values were used for extreme wave analysis for this study. The buoys matching this criterion are located in the North-East and North west of the American continent (north Pacific and north Atlantic). The non-interrupted measurement durations of the used measurements are 40 years at B1 - B3 and 30 years at B4 - B6. Figure 2 shows the positions of those buoys and the locations of all 64 buoys used to validate the wave hindcast data. The total measurement duration interval from the first implementation day to the last used measurements is also presented in Figure 2. All used buoy measurements are filtered based on their quality flag; only the data corresponding to a flag quality value equal to one is considered. The quality information of the Copernicus wave buoy dataset can be found here (De Alfonso et al. 2022).

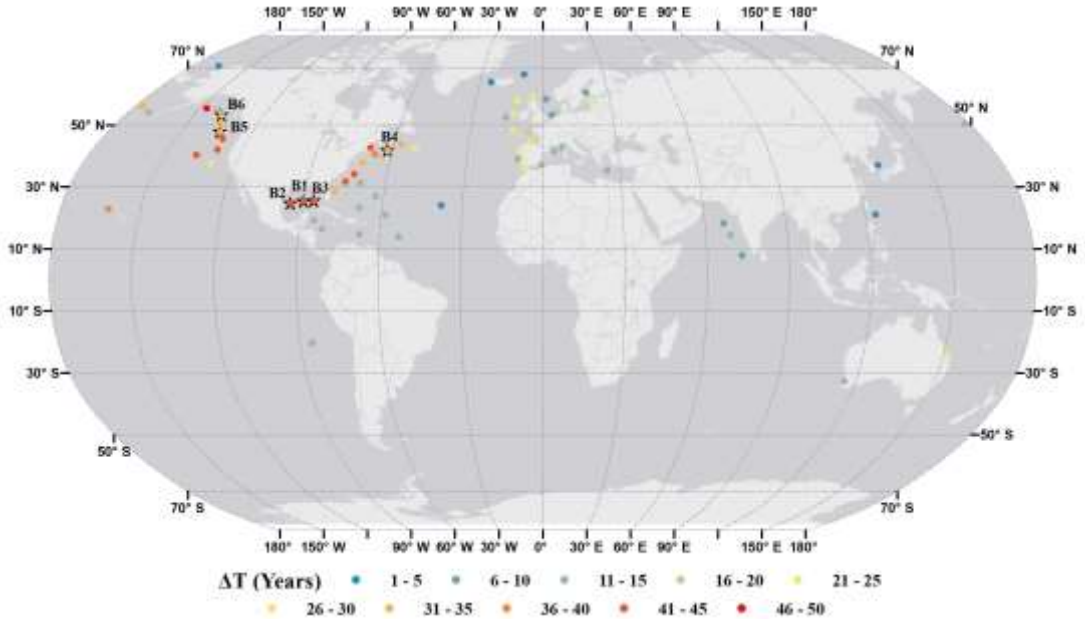


Figure 2. The positions of buoys used in EVA (Star pentagons) and the locations of all 64 buoys used to validate the wave hindcast data (circles) and wave measurement periods at each buoy location are presented with a color gradient.

3.2. SWAN wave hindcasts forced with JRA-55

The Japan Meteorological Agency (JMA) produced JRA-55 Reanalyzes winds (Kobayashi et al. 2015), which is utilized to provide 62-year wave hindcast data. Since JRA-55 covers a longer time than other operational and available reanalyses, it was chosen as the wind-forced model. JRA-55 reanalysis data is available from 1958 to the present. SWAN Cycle III version 41.31 was used to model the JRA-55-based wave hindcast data. The SWAN model has been used to accurately replicate the global wave climate (Yang et al. 2017; Kamranzad and Mori 2019; Liang et al. 2019; Kamranzad et al. 2020, 2022).

The computational and output grid were given priority for such a long-term simulation with the spatial resolution of 1° in both directions since the SWAN model is run with a time step of 30 min. The entire globe is covered by the computation grid, which extends from 90°S to 90°N latitude and 0°E to 360°E longitude. The directional spectral resolution is 10°, and 36 spectral frequency bins range between 0.03 to 1 Hz, with a logarithmic scale. Source terms for the wind field input and nonlinear 4-wave interaction (quadruplets) were taken from the formulations of Komen et al. (1984) and Hasselmann et al. (1985), respectively. Whitecapping source term was calculated using the Komen et al. (1984) formulation, whereas energy dissipation due to bottom friction was computed using the Hasselmann et al. (1973) formulation. The Whitecapping

coefficient (C_{ds2}=2.96e-5) was set to adjust the wave model. It is challenging to calibrate spectral wave models for global simulations since the optimum wave model parametrization varies as a function of the geographic region and geomorphological factors (Amarouche et al., 2021b; Soran et al. 2022). Finally, the General Bathymetric Chart of the Oceans (GEBCO: https://www.gebco.net/), with a spatial resolution of 30 arc seconds, provides the bathymetry input data for the SWAN model. The ice data have not been taken into account as inputs.

The wave parameter output used in this study is the SWH, which is defined based on the zero moments of the energy density spectrum E(f), in which f is the frequency.

$$m_0 = \int_0^{\infty} f^0 E(f)\, df \quad (9)$$

$$SWH = 4\sqrt{m_0} \quad (10)$$

The collected data were validated against offshore wave measurements to perform a careful and reliable assessment of specific potential errors related to wave hindcast accuracy. In-situ measurements are obtained from 64 buoys spread across the globe with recording times (Figure 2). We recognized that a longer measurement time might be more suitable for validation. The largest time span provided by buoy measurements is 1978–2019. Error parameters such as the root mean square errors (RMSE), scatter index (SI), bias, normalized bias (Nbias), and correlation coefficient (R) were determined and presented in Table 1. Thus, for a spatial evaluation of the model accuracy, the correlation coefficient and the bias computed at each buoy were mapped (Figure 1.A).

The wave model slightly overestimates SWH in the North Pacific and Indian Oceans, whereas it slightly underestimates it in the North Atlantic Ocean. The geographic variations in the wave model biases may be attributed to the regional wind climatic regime and/or the precision of the wind field. As the sea surface ice data was not used during the simulation, we can observe a low accuracy of the model results and the highest bias in the Greenland Sea. However, the absolute bias for SWH does not surpass 30 cm at the majority of buoy locations, and the correlation coefficient mainly exceeds 0.88. The average scatter index for SWH equals to 0.29, and the average correlation coefficient is 0.89. These outcomes demonstrate the global accuracy of used wave hindcast data. Additionally, as indicated in the previous section, the wave simulation does not adjust the ice data, which explains why the buoy in the far North Atlantic exhibits the highest biases. Therefore, the results obtained in both the north and south poles are not considered in the discussion, and the accuracy of the results is excluded from the discussions.

345 **Table. 1.** Summary of error statistics determined by comparing the SWAN-JRA-55 SWH
346 estimates to buoy measurements at 64 locations. The bold lines show the buoys with long-
347 term and permanent measurements used for the extreme wave estimates.

Locations	id	Lon (°)	Lat (°)	T_{start}	T_{end}	Data number	R	SI	Nbias	Bias (m)	RMSE (m)	Matching Grid points distances	Coastal distances
Baltic Sea	s1	20.233	61.8	2013	2019	18384	0.91	0.41	0.13	0.15	0.41	0.4	1.04
Baltic Sea	s2	21	59.25	1996	2019	63630	0.93	0.28	-0.09	-0.11	0.35	0.56	0.86
Caribbean Sea	s3	-84.857	19.802	2005	2019	17272	0.91	0.23	-0.1	-0.11	0.28	0.47	2.01
Caribbean Sea	s4	-81.422	16.908	2005	2019	13375	0.88	0.21	-0.01	-0.02	0.27	0.42	2.37
Caribbean Sea	s5	-67.472	15.252	2007	2019	13535	0.84	0.18	-0.05	-0.08	0.29	0.25	2.73
China Sea	s6	124.063	21.677	2012	2016	4297	0.88	0.34	-0.06	-0.1	0.67	0.47	2.35
Chukchi Sea	s7	-167.952	71.758	2012	2015	6366	0.85	0.36	0.13	0.17	0.42	0.52	3.36
Coral Sea	s8	151.071	-23.305	1996	2018	75818	0.88	0.37	0.21	0.22	0.31	0.47	0.16
Greenland Sea	s9	-24.778	65.698	2015	2019	4583	0.9	0.26	0.1	0.3	0.71	0.34	0.35
Greenland Sea	s10	-9.271	68.479	2007	2009	2107	0.91	0.45	-0.5	-1.27	1.73	0.23	2.36
Greenland Sea	s11	-11.401	59.1	1994	2019	31321	0.95	0.21	-0.12	-0.37	0.73	0.41	4.16
Gulf of Mexico	**s12 (B1)**	**-89.66**	**25.84**	**1976**	**2019**	**52602**	**0.86**	**0.37**	**-0.17**	**-0.16**	**0.41**	**0.38**	**3.15**
Gulf of Mexico	**s13 (B2)**	**-94.42**	**25.17**	**1976**	**2019**	**53534**	**0.84**	**0.37**	**-0.23**	**-0.23**	**0.46**	**0.34**	**2.81**
Gulf of Mexico	**s14 (B3)**	**-85.91**	**26.01**	**1977**	**2019**	**50387**	**0.86**	**0.4**	**-0.25**	**-0.21**	**0.43**	**0.64**	**3.53**
Indian Ocean	s15	69.236	14.984	2004	2016	2668	0.86	0.32	0.03	0.06	0.65	0.55	4.36
Indian Ocean	s16	67.103	18.803	2008	2016	2620	0.94	0.33	0.04	0.07	0.53	0.5	3.77
Indian Ocean	s17	73.11	8.486	2008	2016	2791	0.9	0.3	0.1	0.15	0.42	0.39	0.17
Indian Ocean	s18	115.408	-32.094	2004	2017	36247	0.83	0.36	0.21	0.58	0.77	0.42	0.33
Mediterranean Sea	s19	7.8	43.4	2007	2019	17007	0.89	0.38	-0.02	-0.02	0.38	0.32	0.41
Mediterranean Sea	s20	4.683	42.039	2007	2019	16184	0.92	0.35	-0.23	-0.29	0.54	0.5	1.33
Mediterranean Sea	s21	-0.325	37.654	2006	2019	17589	0.88	0.46	-0.51	-0.34	0.47	0.23	0.4
Mediterranean Sea	s22	25.131	35.726	2007	2019	11027	0.88	0.34	0.03	0.03	0.32	0.43	0.34
NE Atlantic	s23	-5.8	48.5	2000	2016	8344	0.91	0.3	0.16	0.36	0.58	0.3	1.04
NE Atlantic	s24	-9.397	42.124	1998	2019	27639	0.9	0.38	-0.35	-0.62	0.9	0.39	0.51
NE Atlantic	s25	-6.963	36.477	1996	2019	30771	0.83	0.46	0.24	0.38	0.56	0.46	0.6
NE Atlantic	s26	-9.64	39.51	2009	2019	8455	0.9	0.23	0.02	0.04	0.53	0.14	0.32
NE Atlantic	s27	-15.73	53.182	2006	2019	15805	0.94	0.2	-0.06	-0.18	0.66	0.39	5.44
NE Atlantic	s28	-5	45.2	1998	2019	27677	0.94	0.22	-0.08	-0.18	0.55	0.58	1.68
NE Atlantic	s29	-12.401	48.701	1991	2019	32334	0.93	0.23	-0.12	-0.35	0.73	0.22	3.69
NE Atlantic	s30	-12.367	54.55	1993	2017	27424	0.94	0.22	-0.12	-0.35	0.75	0.14	2.18
NE Pacific	s31	-148.17	56.3	1974	2019	59064	0.82	0.31	0.06	0.17	0.83	0.39	3.51
NE Pacific	s32	-130.36	42.58	1975	2019	48931	0.81	0.31	0.08	0.25	0.82	0.16	5.83
NE Pacific	s33	-136.095	50.93	1988	2019	32241	0.92	0.24	0.07	0.21	0.67	0.59	4.11
NE Pacific	s34	-131.02	46.05	1976	2019	47981	0.83	0.32	0.09	0.26	0.86	0.66	5.16
NE Pacific	s35	-137.48	40.8	1977	2019	41357	0.85	0.31	0.08	0.24	0.86	0.3	12.88
NE Pacific	s36	-177.58	57.05	1985	2019	38330	0.93	0.25	0.1	0.28	0.66	0.46	5.14
NE Pacific	**s37 (B5)**	**-133.938**	**48.355**	**1987**	**2019**	**38374**	**0.91**	**0.25**	**0.06**	**0.19**	**0.71**	**0.46**	**4.62**
NE Pacific	s38	-129.898	38.05	1994	2019	27113	0.89	0.25	0.06	0.16	0.67	0.6	5.99
NE Pacific	s39	-171.981	55.011	2005	2019	11640	0.93	0.3	0.17	0.5	0.76	0.69	2.65
NE Pacific	s40	-142.492	55.868	2007	2019	11967	0.93	0.24	0.04	0.12	0.63	0.37	4.17
NE Pacific	**s41 (B6)**	**-138.85**	**53.915**	**1987**	**2019**	**36107**	**0.92**	**0.24**	**0.07**	**0.22**	**0.65**	**0.54**	**4.34**
NE Pacific	s42	-162.21	23.43	1981	2019	39631	0.83	0.23	0.06	0.15	0.55	0.3	2.51
North Sea	s43	6.333	55	1993	2012	10265	0.93	0.23	0.01	0.02	0.42	0.53	1.43
North Sea	s44	1.5	59.5	2011	2019	10559	0.92	0.23	0.05	0.14	0.54	0	2.61
North Sea	s45	-4.5	60.701	1999	2019	22162	0.93	0.22	-0.08	-0.24	0.67	0.2	1.97
North Sea	s46	4.016	54.117	2011	2019	75429	0.94	0.23	0.05	0.08	0.36	0.62	1.25
NW Atlantic	s47	-72.66	34.68	1976	2019	40139	0.81	0.36	-0.16	-0.27	0.73	0.24	2.91
NW Atlantic	s48	-75.42	32.27	1975	2019	44057	0.84	0.32	-0.11	-0.18	0.58	0.24	2.61
NW Atlantic	s49	-78.55	28.9	1988	2019	48378	0.91	0.26	-0.14	-0.19	0.41	0.4	2.02
NW Atlantic	s50	-53.024	14.516	2005	2019	17186	0.82	0.17	-0.09	-0.16	0.34	0.48	6.55
NW Atlantic	s51	-58.625	21.575	2009	2019	13898	0.87	0.19	-0.07	-0.12	0.35	0.15	5
NW Atlantic	s52	-68.417	23.832	2007	2019	15756	0.86	0.22	-0.07	-0.11	0.38	0.34	3.81
NW Atlantic	s53	-69.59	31.86	2007	2019	15578	0.94	0.23	-0.07	-0.12	0.43	0.37	4.75
NW Atlantic	s54	-62.945	27.537	2009	2019	14201	0.91	0.21	-0.06	-0.1	0.39	0.45	5.08
NW Atlantic	s55	-38	24.581	2012	2013	1566	0.84	0.2	0.03	0.08	0.42	0.51	14.71
NW Atlantic	s56	-70.56	38.47	1977	2008	34397	0.82	0.37	-0.11	-0.2	0.75	0.07	2.82
NW Atlantic	s57	-69.18	43.18	1978	2019	45521	0.82	0.37	0.04	0.07	0.56	0.45	0.79
NW Atlantic	s58	-66.62	41.11	1984	2019	38045	0.9	0.31	-0.13	-0.23	0.63	0.41	2.6
NW Atlantic	**s59 (B4)**	**-61.998**	**42.262**	**1988**	**2019**	**28265**	**0.91**	**0.29**	**-0.1**	**-0.2**	**0.68**	**0.55**	**2.52**
NW Atlantic	s60	-57.103	44.24	1988	2019	25055	0.93	0.24	-0.04	-0.08	0.54	0.47	2.63
NW Atlantic	s61	-51.467	42.868	1990	2012	17869	0.91	0.22	0.02	0.06	0.56	0.37	4.13
NW Pacific	s62	179.001	51.155	2004	2017	8005	0.89	0.32	0.09	0.26	0.85	0.61	0.31
SE Pacific	s63	-85.567	-19.691	2007	2018	13825	0.81	0.23	0.14	0.36	0.52	0.2	10.82
Sea of Japan	s64	131.11	37.46	2011	2016	1575	0.92	0.32	-0.22	-0.28	0.49	0.39	0.19

348

349

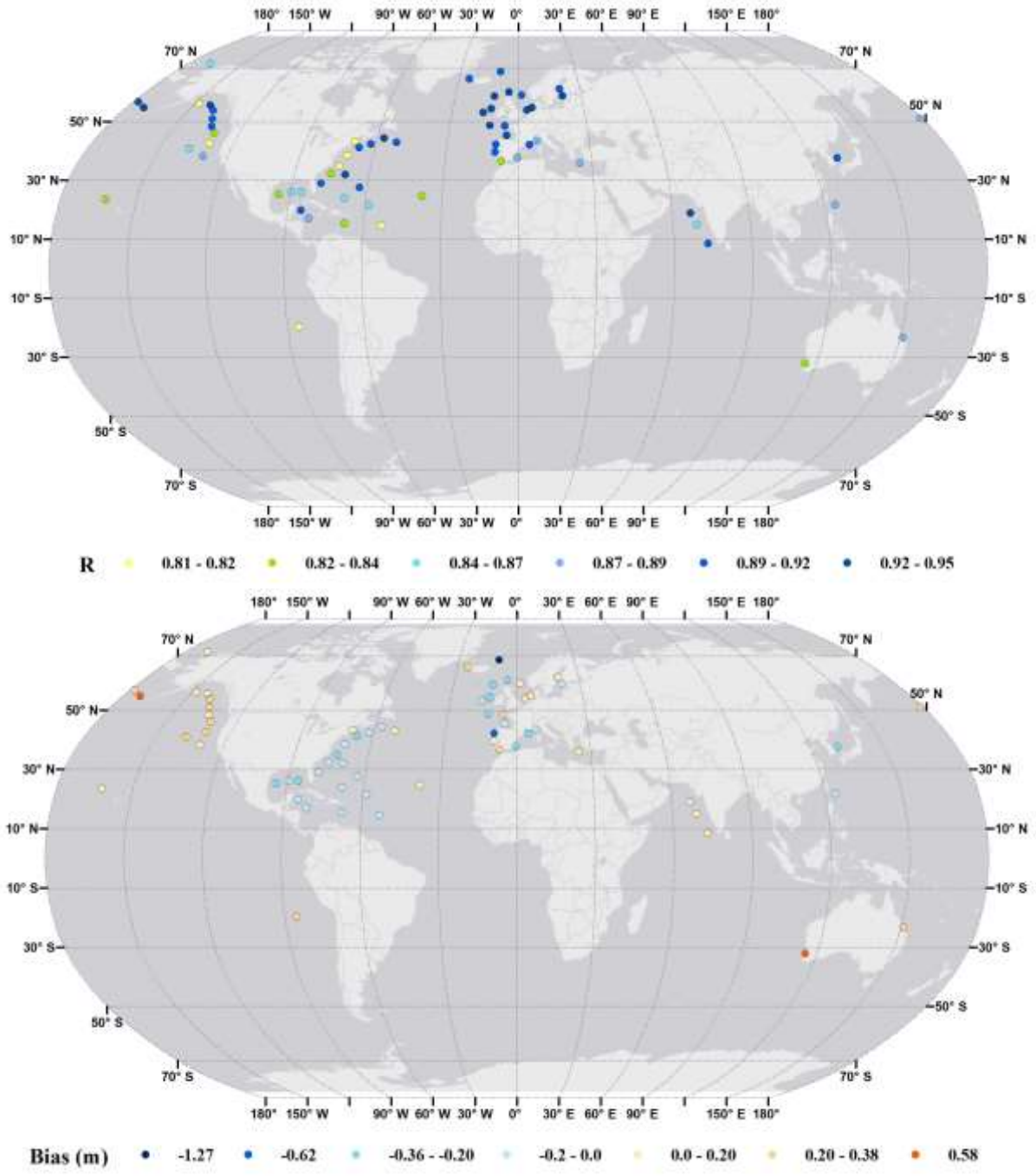


Figure 1. A. Correlations (Up) and biases (Down) in SWH computed at each buoy for SWAN-JRA-55 hindcast. The star pentagons show the buoy locations used in extreme value analysis and other buoy locations, respectively.

3.3. ERA5 wave hindcasts

The ERA5 reanalysis is a recent version updating the ERA-Interim by adding and adjusting various attributes and using the latest version of the Integrated Forecasting System (IFS Cycle

41r2) to develop ERA5 assimilation system. In comparison to ERA-Interim, ERA5 has increased the Spatio-temporal resolution for wind modeling from 6 hours to hourly and from 80 km grid resolution with 60 vertical levels up to 0.1 hPa (Dee et al. 2011) to 31 km with 137 levels up to 0.01 hPa in ERA5 (Hersbach et al. 2020). Improvement in the wind reanalysis data leads to improvement in the reanalysis of the ocean waves. The atmosphere causes ocean waves through surface wind stress and affects the atmospheric boundary layer through sea-state dependencies in the surface roughness. Besides that, the resolution of the ocean wave model is increased from 1^{o} in ERA-interim to 0.360^{o} for hourly data. However, it should be noted that the ERA5 is supplied for a 0.5^{o} interpolated grid. The optimal interpolation is carried out hourly in ERA5 rather than six hours as in ERA-Interim to match the hourly output of ERA5. The scatterometer and altimeter satellite observations are used to perform the wave output adjustment for the ERA5 ocean wave simulation. During the ERA5 implementation, altimeter measurements of SWH were employed, taking into account observations till the 1991 launch of ERS-1. The products from ERS-1/-2, Jason-1, and Envisat are reprocessed as well as those of ERS-1/-2, Jason-1, and Envisat. ERA5 wave data was evaluated and validated by (Hersbach et al. 2020).

3.4. Satellite observations

The satellite altimeter observations used during this study were provided by the Satellite Research and Exploitation Centre (CERSAT). This satellite dataset is a multi-platform altimeter product produced at IFREMER as part of the GlobWAVE project. Detailed information about the used dataset is presented in (Queffeulou and Croize-Fillonr 2017). The IFREMER altimeter dataset is developed based on the following satellites: ERS-1, ERS-2, GEOSAT FO, TOPEX/POSEIDON, JASON-1, JASON-2, ENVISAT, Cryosat-2, SARAL/AltiKa. The SWH data obtained from those missions were all corrected against wave-buoys measurements. The equation used for the altimeter data correction can be found in (Queffeulou and Croize-Fillonr 2017). Thus, the accuracy of each used satellite data was validated in several studies against buoy measurements worldwide, e.g., the CryoSat-2, was evaluated by (Abdalla et al. 2018), showing a correlation coefficient >0.98 between CryoSat-2 SWH observations and wave measurements from seven buoys located in the North Atlantic. For SARAL/AltiKa data, Hithin et al. (2015) have reported that the SWH observed from SARAL/AltiKa satellite agrees well with the in-situ measurements with a high correlation of 0.98. The altimetry observation obtained by ENVISAT and Jason-1 was also validated compared to buoy measurements

(Durrant et al. 2009), showing a correlation coefficient of 0.98. The accuracy assessment of the SWH obtained by TOPEX/POSEIDON mission is presented in (Lee-Lueng Fu 1994; Leben and Powell 2010). Furthermore, using cross-altimeter and buoy comparisons (Queffeulou 2010), we performed a long-term validation of the wave height data set provided by ERS, TOPEX/Poseidon, GEOSAT Follow-on, Jason-1, and ENVISAT.

The IFREMER satellite altimeter data cover the period from 1991 to 2017. In the present study, we used 20 years of data from January 1st, 1995, to December 31st, 2016. The data for 2017 was not considered as they are not covering all years, and data from 1991 to 1994 are of low spatial and temporal density. The data was spatially grouped using a regular global grid of 1^{o} x 1^{o}. For the AM-GEV model, the yearly maximum SWHs observed at each cell were determined for the used 20-year period. For the application of the POT-GPD model. The whole data observed at each cell was considered for estimating the threshold. Thus, the observation exceeding the threshold was filtered by considering a minimum duration between two successive peaks of 48h.

4. Results and discussions

In the present study, the resources and periods compared are of four different natures (Satellite, buoys, reanalyzes, and hindcast) and cover a longer period. Thus, an automatic objective method is used to determine the thresholds for the POT -GEV model. On the other hand, the goodness of fit of each data set and in each point of the globe are determined for GPD and GEV distributions. Also, the accuracy of the estimated distribution parameters is evaluated in terms of the upper confidence interval for a 95% confidence level. A wide confidence interval reflects a higher uncertainty in the estimates of extreme values.

Currently, the studies on global extreme SWH are limited, and the most common are (Vinoth and Young 2011; Young et al. 2012; Yang and Oh 2018; Takbash and Young 2019; Lobeto et al. 2021). Those studies have been developed to estimate extreme waves on a global scale based on wave data from various sources and for different periods. The results of the mentioned studies provide different values of the estimated extreme SWHs for the same return period of 100 years. On the other hand, in a few studies (Cai and Hames 2010; Orimolade et al. 2016), the target objectives were in line with those of the present study. This section consists of the comparison of the results of previous studies where appropriate.

4.1. AM-GEV model results

The accuracy of the estimated extreme SWH values may depend on the estimated distribution parameters and the goodness of fit of the analysed dataset against the used distribution model. Therefore, we start firstly by assessing the accuracy of the estimated distribution parameters based on the confidence interval values of both shape and scale parameters. After that, to assess the sensitivity of the different returned-period extreme SWHs estimated to the used data sources and the used data periods at a global and spatial scale, we compared the extreme SWH results for 100 years return period. Finally, the accuracy of the extreme waves estimated based on the reanalysis ERA5 and hindcast SWAN-JRA-55 data versus those of the measurements was investigated.

4.1.1. Accuracy of distribution parameters and Goodness of fit

Figures 3 and 4 show an important variation in the confidence interval (CI) of the estimated shape and scale parameters. The confidence interval is reduced by increasing the analysed duration and so by increasing the sample size. However, an exception is observed in the Tropical North Pacific (TNP) off Mexico coasts using the wave hindcast data (SWAN-JRA), where the confidence interval of the estimated scale parameters has increased by increasing the analysed period. By comparing the results obtained using different data sources, we noticed that the highest CI values in both scale and shape parameters are obtained using satellite observation. Besides, using a short period of 10 years, the CIs of the distribution parameters estimated for satellite observations are spatially more homogeneous and lower than those obtained using the hindcast (SWAN-JRA-55) and the reanalysed dataset (ERA5). For a period of 20 years, CIs are close to each other for three data sources for the estimated shape parameter, but remarkable differences are observed in CIs of the estimated scale parameter. The estimates appeared more accurate using the hindcast data. Thus, the main differences are observed in the TNP, specifically in the North Philippines Sea. The highest CI values of scale parameter are observed in the Philippines Sea, followed by the extra-tropical north Atlantic (ETNA) region. Thus, in the West Tropical North Atlantic (TNA) CIs of the shape and scale parameters are more important using the ERA5 reanalysed dataset of 20 years. Using a 40-year dataset, the CI values for wave hindcasts (SWAN JRA-55) are close to those obtained using ERA5 reanalysed. Using a 60-year dataset, we noticed an improvement in CIs of both shape and scale parameters,

except in the North Philippines Sea and off Mexico coasts, as mentioned previously. The wave climate regime in these two locations may not be appropriate for a GEV distribution model.

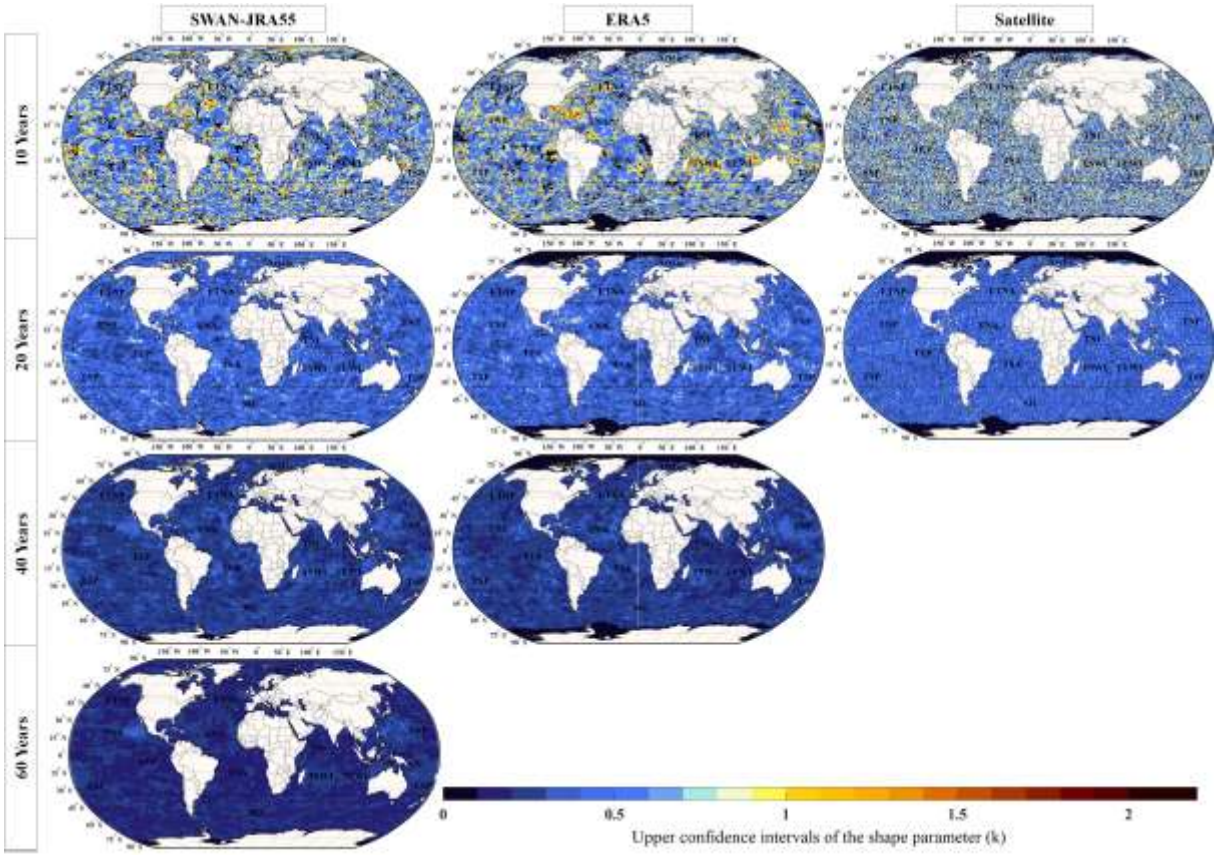


Figure 3. Map showing the upper confidence intervals of the shape parameter (ξ) estimated using the MLE method for SWAN-JRA-55 wave hindcast data (the first column), the reanalysed ERA5 wave data (the second column), and satellite observation data (third column) fitting the GEV distribution. Each row corresponds to a distinct period from 10 to 60 years.

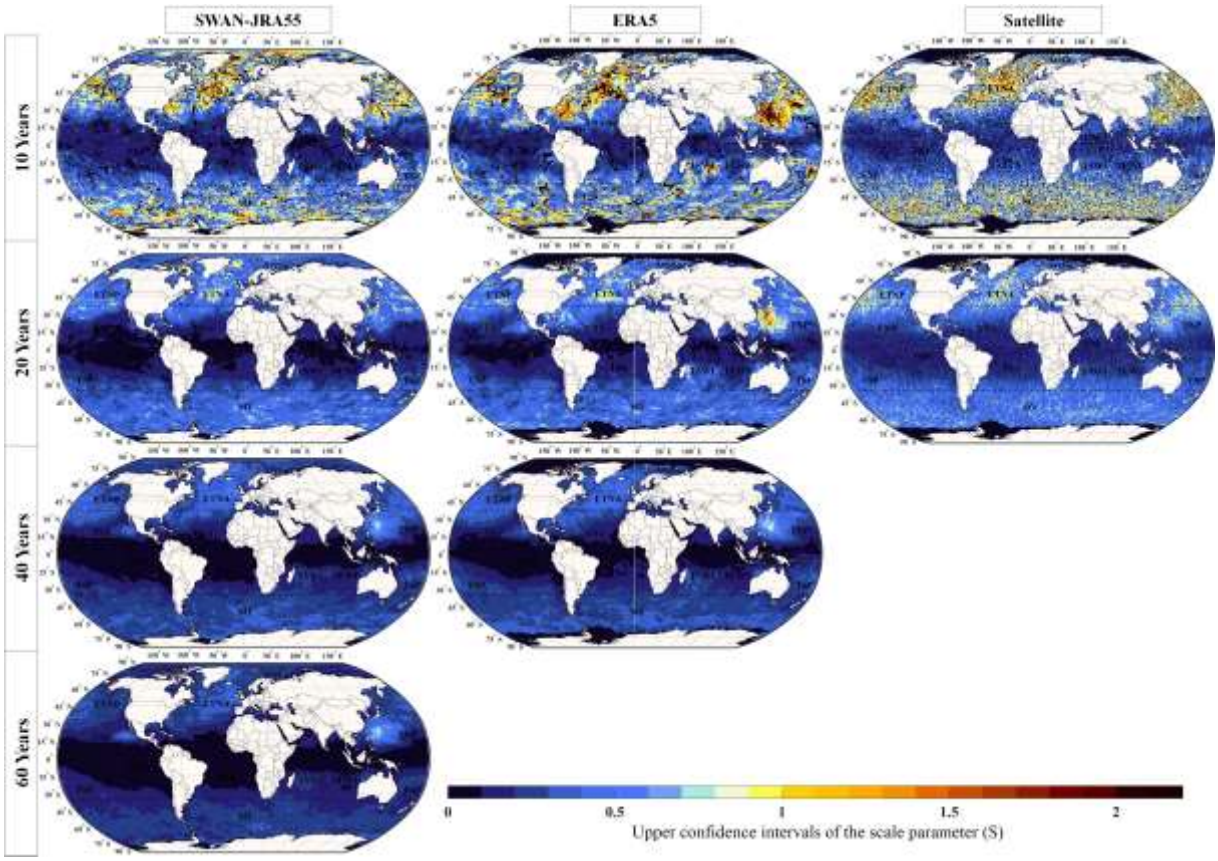


Figure 4. Map showing the upper confidence intervals of the scale parameter (σ) estimated using the MLE method for SWAN-JRA-55 wave hindcast data (the first column), the reanalysed ERA5 wave data (the second column), and satellite observation data (third column) fitting the GEV distribution. Each row corresponds to a distinct period from 10 to 60 years.

By evaluating the goodness of fit of the used dataset against the GEV distribution (Figure 5), we noticed that all used datasets present a significant fit to the GEV distribution at a risk level alpha=0.05, and in the majority of the global offshore seas. However, a non-significant fit is observed in the near coast areas using the wave hindcast data. Thus, using the reanalysis data, a non-significant fit is also noticed in the Polar Regions for satellites and in a larger polar area. The results in this location are not discussed for the hindcast data considering that the ice information was not used during the wave hindcast simulation. It is essential to notice that the satellite dataset fits the GEV distribution in the Polar Regions more closely, with a lower CI for the shape and scale parameters. This result may be explained by the fact that satellite tracks and observations are denser in the polar regions than in the regions located far from the poles.

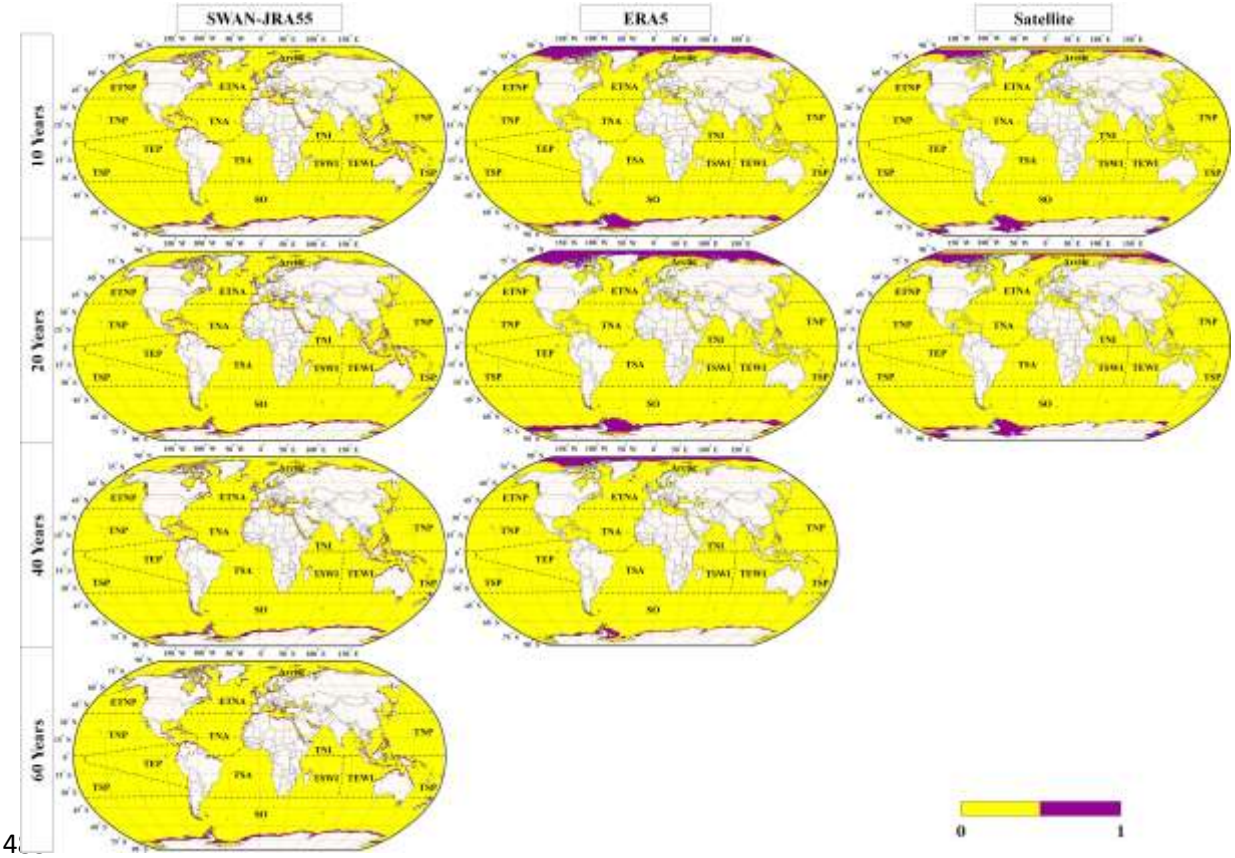


Figure 5. Map showing K-S test hypothesis results. In the yellow areas, the null hypothesis H_0 is maintained (The Annual-maxima data fit GEV distribution) at a risk level alpha=0.05, while in the purple areas, the null hypothesis H_0 is rejected. The results shown fit the SWH data from SWAN-JRA-55 hindcast (the first column), the ERA5 reanalysis (the second column), and the satellite observation (the third column). Each row corresponds to a distinct sample size from 10 to 60 years.

4.1.2. Extreme SWH estimates

To assess the sensitivity of the extreme SWHs estimated to the used data sources and to the used data periods at a global and spatial scale, we are comparing the extreme SWH results for 100 years returned period. The extreme SWHs discussed here are estimated using the AM-GEV for each dataset. In the first overview (Figure 6), we notice that return waves exceeding 30 m are evaluated in some tropical regions. Furthermore, the highest CIs in shape and scale parameters are estimated for those regions (Figure 3,4). Those results are considered outlier anomalies in the present study. However, those outlier anomalies are less observable when using satellite data.

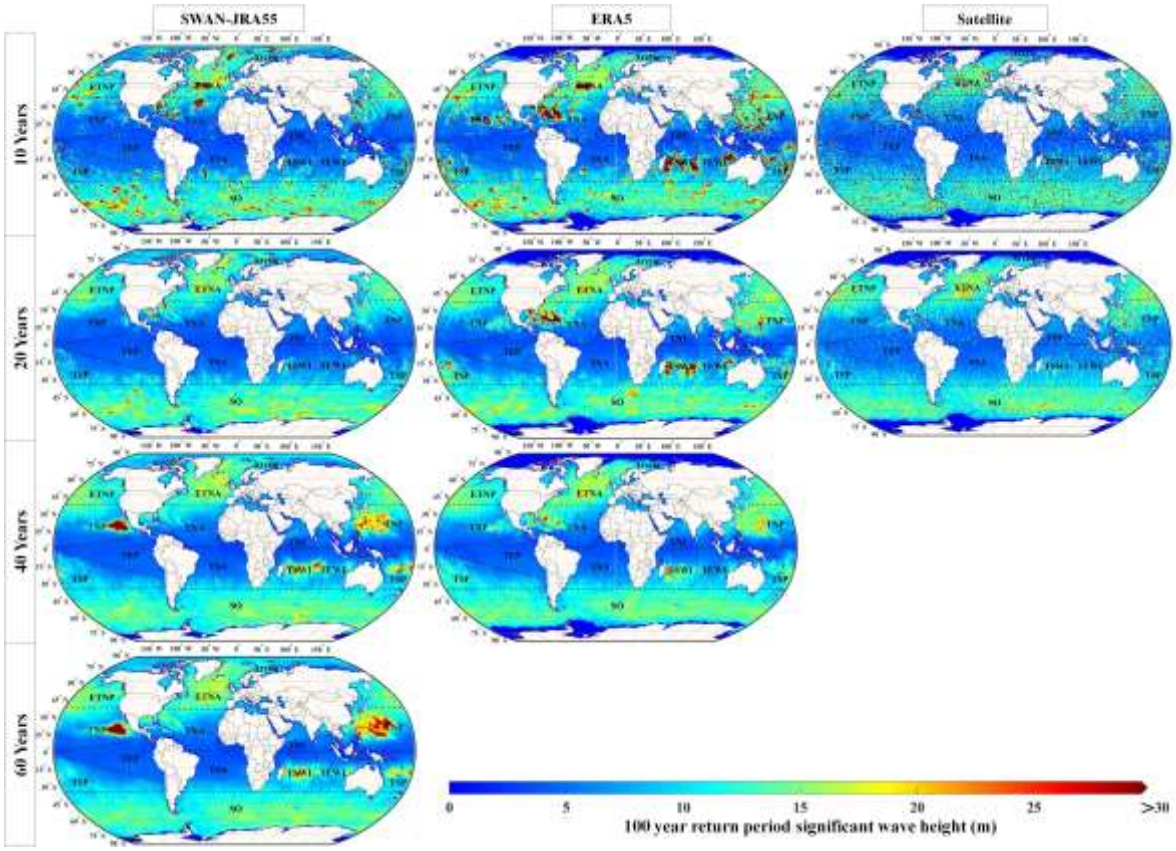


Figure 6. Extreme SWHs with a 100-year return period estimated using AM-GEV model for SWAN-JRA-55 wave hindcast data (the first column), the ERA5 wave data (the second column), and satellite observation data (the third column). The maps in each row correspond to a distinct period from 10 to 60 years.

The K-S test reflects a good fit considering the theoretical wave distribution fitted based on the estimated shape and scale parameters. However, the uncertainty in the estimated shape and scale parameters using the MLE method is high in tropical cyclone regions. The goodness of fit does not always reflect the accuracy of the estimated extreme values. Furthermore, geographically speaking, as the observed outliers are located in regions characterized by the highest density of tropical cyclones (O'Grady et al. 2022), the overestimated results may depend on the accuracy of tropical cyclone estimates provided by ERA5 and JRA-55 reanalyses. In areas of low cyclone activity, the overestimation is only observed using the dataset of a short period (10 years). The results based on ten years of data also present larger confidence intervals in the estimated shape and scale parameters (Figures 3 and 4). Based on ten years of data, the results are more acceptable when using satellite observations. Comparing the results obtained from satellite, SWAN-JRA55 hindcast, and ERA5 reanalysis for the same data period of 20 years, we observed that the relative differences depending on the used data sources are computed and shown in (Figure 7 (a-c)). In the regions of tropical cyclone activities,

524 the absolute relative differences can reach 80% comparing SWAN-JRA55 results to satellite
525 data results (Figure 7 (a)), and reach 100% comparing ERA5 results to satellite data results
526 (Figure 7 (b)). The extreme SWH results obtained using ERA5 data are overestimated compared
527 to those obtained based on satellite data in the northern and southern tropical regions and
528 underestimated in the tropical region. Using SWAN-JRA55, the relative changes out of the
529 regions of tropical cyclone activities are mainly <20% compared to both ERA5 and satellite
530 results (Figure 7 (a,c)). The extreme SWH is overestimated compared to those obtained based
531 on satellite data in the North Atlantic and southern ocean and underestimated in most of the
532 remaining global oceans. Using SWAN-JRA55, the highest relative differences are observed in
533 the west tropical Atlantic, with and underestimation of >60% (Figure 7 (a)).

534 By increasing the analysed ERA5 data period to 40 years, areas with extreme SWH values
535 estimated to exceed 30 m are adjusted using the ERA5 reanalysis data (Figure 6), unlike the
536 result obtained from the SWAN-JRA-55 hindcast dataset, showing an increase in outlier values
537 over the southern Indian Ocean and in the eastern and western Pacific tropics. Low accuracy in
538 some tropical cyclones occurring over the Northeast Pacific and the North Atlantic from 1959
539 to 1987 reported by the Japan Meteorological Agency (2020), can explain the overestimated
540 extreme values. Thus, Murakami (2014) showed that the estimates of the tropical cyclone in
541 JRA-55 reanalysis data are more accurate in 1979-2012 compared to the 1958-2012 period.
542 However, Murakami (2014) also reported that regarding the spatial distribution of tropical
543 cyclones, highest hitting rate, lowest false alarm rate, reasonable tropical cyclone structure, and
544 representation of inter-annual change in tropical cyclone frequency, the JRA-55 appears to be
545 the best reanalysis. The data's long-term accuracy is also important and may significantly affect
546 the results in tropical regions. In global wave climate studies, particular focus should be devoted
547 to the NE tropical Pacific and the Philippine Sea. The density of tropical cyclones in these
548 specific areas can be considered the highest in the world based on the results of Vecchi et al.
549 (2014). The accuracy of the maximum wave value estimated in this region may be influenced
550 by the lack of accuracy in estimating the wind forcing during tropical cyclones. Considering
551 more peak events at the tropical cyclone location may be more accurate for extreme wave
552 analysis. Thus, a POT model can be more appropriate at those locations.

553 Outside of these tropical cyclone regions, relative changes are exceeding 10% in large part of
554 the globe, comparing the extreme SWHs estimated based on ten years of SWAN-JRA55 and
555 ERA5 data to those estimated based on 20 years ((Figure 7 (d, f)). Using the satellite data, the
556 relative change as a function of the used data period are mainly >20% (Figure 7 (g)). By

increasing the analysed data period of ERA5 and SWAN-JRA55 to 40years, the relative changes rarely exceed 10%, except in tropical cyclone regions (Figure 7 (g, h)). The results remain close by increasing the analysed period to 60 years in the case of the SWAN-JRA-55 data (Figure 7 (i)). Using the AM-GEV model, the increase in the analysis period beyond 20 years did not lead to a notable change in the estimated extreme SWH values over a large part of the globe. However, depending on the data source, the increase in the period may correct the errors in cyclonic regions and decrease the confidence intervals.

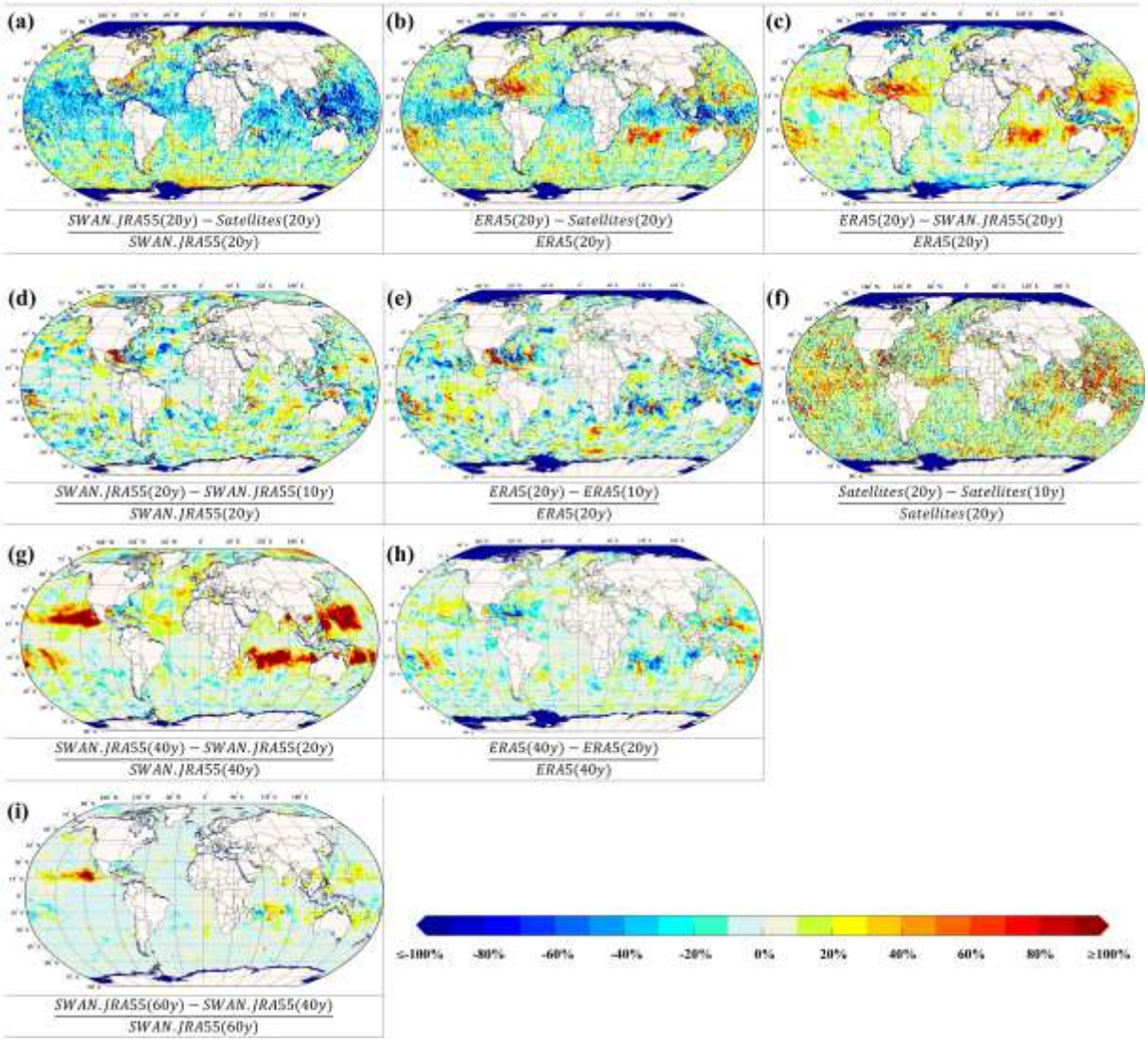


Figure 7. Maps showing the relative biases calculated by comparing the extreme significant wave height of the 100-year return period estimated using the AM-GEV on the basis of different analysed data periods and different data sources. The maps a-f show the biases when comparing the results obtained from different data periods within the same data source, and the maps h-j show the biases between the results obtained from three data sources for the same period of 20 years (20y).

572 The AM-GEV approach does not depend on an estimated threshold or time limit between two
573 peaks, which allows a more precise comparison of the obtained results. However, to the limit
574 of our knowledge, no recent global studies on extreme waves have been performed based on
575 the AM-GEV approaches until now. However the results obtained based on satellite observation
576 are in line with those of (Aarnes et al.) in the North Atlantic Ocean using the AM-GEV
577 approaches. The estimated extreme SWH in the North Atlantic Ocean reached 20 m for a return
578 period of 100 years. Thus, on a global scale, the results are also in line with those obtained using
579 satellite observations (on a 1◦ × 1◦ grid) and POT-GPD approach by (Vinoth and Young 2011)
580 and close to those of (Takbash and Young 2019) and (Takbash et al. 2019).

581

582 **4.1.3. Accuracy of the estimated extreme SWHs**

583 Extreme SWHs are estimated at six buoy locations, where we can compare the results obtained
584 using buoy measurements and those obtained using reanalysed ERA5 dataset and the SWAN-
585 JRA-55 hindcast dataset at the nearest grid location to the buoys (Figure 8). The considered
586 buoys are located offshore and provide real-time measurements without interruptions for an
587 extended period. The extreme SWHs for different return periods are estimated, and the
588 confidence interval at each estimated value was computed for the risk of alpha of 5%. This
589 comparison aims to evaluate the sensitivity of the estimated extreme SWHs to the unused data
590 sources at different return periods. The comparison against the satellite data is subjective, noting
591 that satellite observation data at the exact location depends on the satellite duration cycle and
592 the number of satellites tracked at the same locations. The satellite observation misses several
593 peaks of the storm events, which conduce an underestimation of the extreme SWH compared
594 to the buoy measurements. We consider that the most accurate results are those obtained based
595 on buoy measurements. Using the buoy measurements, the goodness of fit on each dataset may
596 provide an idea about the accuracy of the estimated extreme waves. The K-S test was applied
597 to each dataset (Table 2). The results show that all datasets are significantly fitting the GEV
598 distribution. The results obtained using both reanalysed ERA5 and wave hindcast of SWAN-
599 JRA-55 are different from those obtained based on buoy measurements. The confidence interval
600 in the Gulf of Mexico is larger considering ERA5 and SWAN-JRA-55 datasets. We can notice
601 that the extreme SWHs estimated based on ERA5 and SWAN-JRA-55 datasets are
602 underestimated for the returned period < 10 years but overestimated for a returned period > 10
603 years compared to the buoy measurement results.

604

605 **Table 2**. P-values obtained as results of the K-S test for buoy measurements and their
606 corresponding ERA5 and SWAN-JRA-55 datasets. The null hypotheses are rejected if the p-
607 value<0.05

Data sources → Locations	**Buoys**	**ERA5**	**SWAN-JRA-55**
B1	0.82	0.24	0.13
B2	0.49	0.78	0.54
B3	0.80	0.71	0.73
B4	0.27	0.32	0.95
B5	0.81	0.95	0.69
B6	0.86	0.19	0.47

608

609 The extreme SWH estimated for 100 year return period at B1 - B3 are close to those obtained
610 by Jeong and Panchang (2008) using the same approaches at the same buoys. Those three buoys
611 are identified as 42001, 42002, and 42003 successively in Jeong and Panchang (2008). At B4 -
612 B7, the results obtained using ERA5 and SWAN-JRA-55 are underestimated compared to the
613 buoy measurement results for all evaluated return periods. Even considering the confidence
614 interval band, the results remained far from the measurements-based results, except for the
615 return period >20 years at B5 and the return period < 10 years at B6. The underestimation of
616 the extreme event peaks of both ERA5 and SWAN-JRA-55 hindcasts can explain these results.
617 The SWAN-JRA-55 hindcast biases computed by considering the whole data are positive in the
618 NE Pacific. However, the calibration and validation of wave models are based on the whole
619 data and not on extreme data. Amarouche et al. (2021a) showed that a calibrated SWAN model
620 forced by ERA5 wind underestimates the storm peaks and that the model parameters may be
621 optimized to obtain a more accurate estimation of peak events at a regional scale.

622 Taking into account that the AM-GEV method results do not depend on the threshold selection,
623 the results show the high sensitivity of the estimated extreme SWH to the accuracy of the used
624 data sources. The hindcast and reanalysed data are validated based on buoy measurements and
625 show an acceptable accuracy considering the whole data. However, their accuracy in estimating
626 the annual maxima in SWH is not commonly evaluated. The overestimation of extreme SWH
627 may economically affect offshore and marine activity. Thus, their underestimation may also
628 lead to a non-durable infrastructure designed in the coastal and offshore regions and engender
629 as well economic effects and considerable risks.

630 Using the AM-GEV, the estimated return period using ERA5 reanalysed and SWAN-JRA-55
631 hindcast may provide biased results with larger confidence intervals. These results show the
632 importance of increasing the buoys measurement worldwide and the improvements in the

accuracy of the existing models in estimating the SWH peaks during storm and tropical cyclone events. Using a calibrated wind wave model at a higher spatial resolution on a local scale may provide better estimates of the extreme wave return periods. However, the global model hindcast and reanalysis data are not recommended for extreme wave analysis based on AM-GEV for coastal and offshore engineering projects. The use of satellite data can provide a more accurate alternative; however, satellite data are limited in time and space. Some yearly storm peaks can be missed in satellite observations depending on the time matching of the satellite track. Therefore, using AM-GEV model, the results obtained for satellite data could be underestimated, as shown in the spatial results (Figure 6) and as shown by Alves and Young (2003).

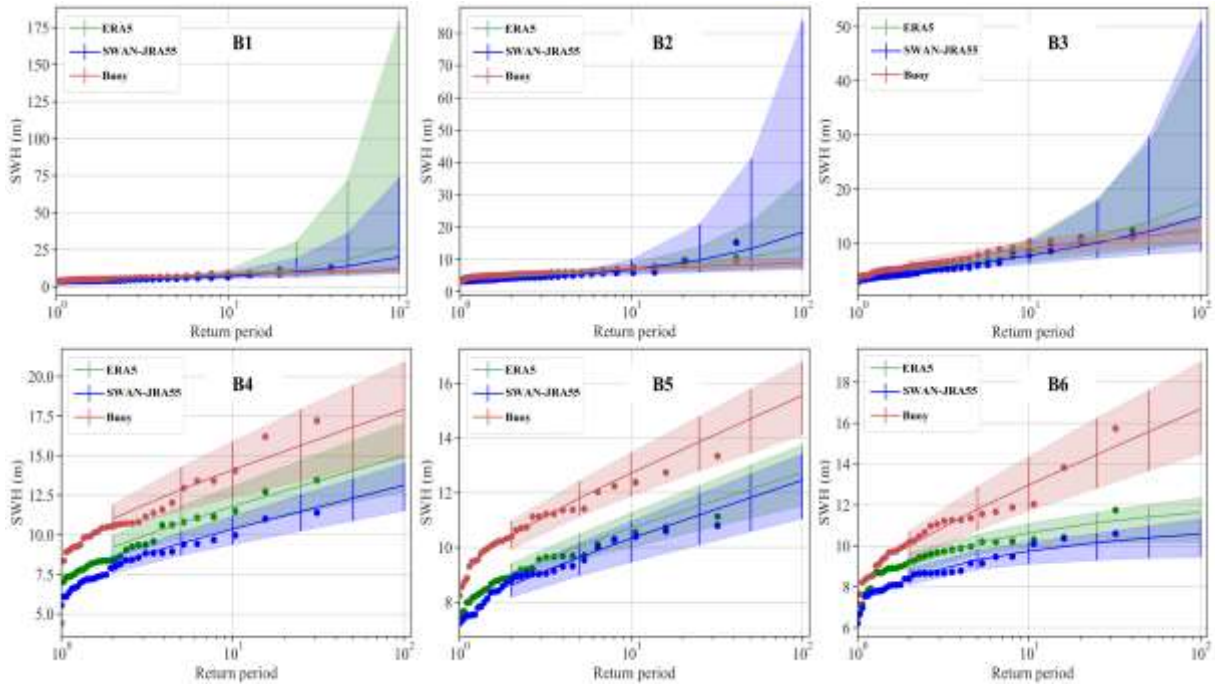


Figure 8. Extreme SWHs at different return periods estimated using an AM-GEV model at six buoy locations based on wave measurements, SWAN-JRA-55 wave hindcast, and ERA5 wave reanalyze. The shaded color shows the confidence intervals for the risk of α=0.05.

4.2. POT-GPD model results

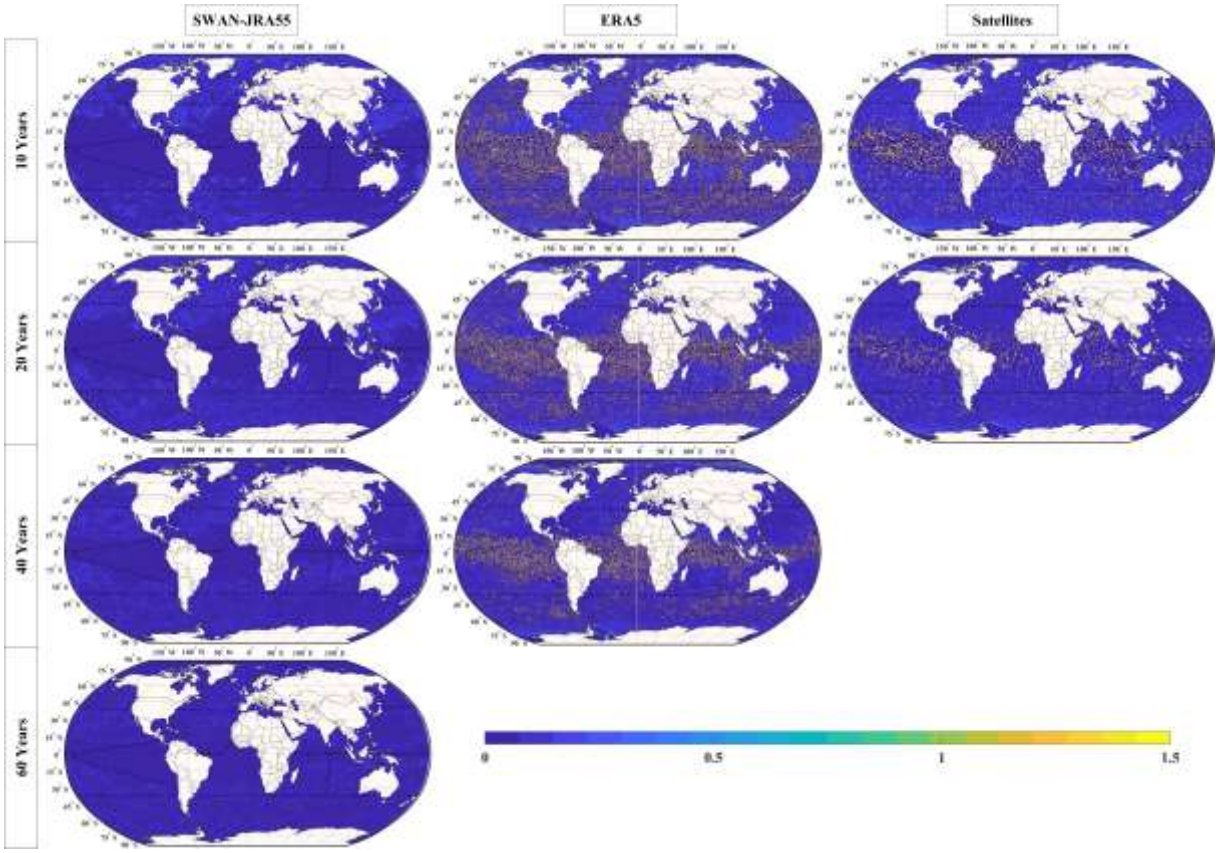
4.2.1. Distribution Parameter Accuracy and Goodness of Fit

Referring to the computed confidence intervals (CIs) values of both shape and scale parameters, the accuracy of the estimated distribution parameters was discussed. CIs are computed for a

confidence level of 95%. Figures 9 and 10 show the spatial variation in the CI of the estimated shape and scale parameters as a function of the data sources and the considered period. By increasing the analysed duration, it is observed that the CIs are reducing at a global scale. Using ERA5 data and satellite observations, the shape parameters in the tropical zones are estimated with the highest CIs values. However, by increasing the used duration, the CIs are reduced. Using the SWAN-JRA-55 hindcast data, the CIs of the estimated shape parameter is lower on a global scale. The CIs for GPD parameters are more homogeneous and varying as a function of altitude, contrary to the results obtained for the GEV estimated parameters. Concerning the scale parameter, a more considerable difference in the results was obtained using different sample sizes. The CI for the estimated scale parameters is more prominent using ten years of data in the North Atlantic, North Pacific, and Southern Ocean locations. The lowest CIs for the estimated scale parameter can be observed for the SWAN-JRA-55 and ERA5 datasets of 60 and 40 years successively, except in the Southern Indian Ocean, where the CIs slightly increase by increasing 40- and 60-year SWAN-JRA-55 data. The CIs in the Southern Ocean are lower using 20 years of the SWAN-JRA-55 dataset. The highest CI values in both scale and shape parameters are obtained using the 10-year ERA5 dataset. For both GEV and GPD distributions, satellite observations of a short period (10 years and 20 years) may provide lower uncertainty in the estimated distribution parameters compared to the ERA5 reanalysis and SWAN-JRA-55 dataset for the same period.

The goodness of fit test (K-S test) is performed on different datasets fitted against the GPD distribution, and the obtained hypotheses are mapped (Figure 11). The results show that for 10- and 20-year periods, datasets exceeding the selected threshold have a significant fit to GPD in most of the globe. However, by increasing the analysed period to 60 years using the SWAN-JRA-55 dataset, a larger area in the Indian Ocean and the tropical Pacific show no significant fit to GPD. The increase in the areas of no significant fit by increasing the analysed period is also observed with both ERA5 and satellite datasets. However, the area of non-significant fit is extremely small using those two data sources. The K-S test applied to the ERA5 dataset exceeding the selected thresholds shows a significant fit to GPD in most of the globe for all analysed periods of 10, 20, and 40 years. Only some small areas in the polar regions in the South Indian Ocean show a non-significant fit using the 40-year ERA5 dataset. Using the satellite observations of 10 and 20 years, the area of non-significant fit is larger in Polar Regions and also increases by increasing the analysed period. Thus, several grid points worldwide show no significant fit using satellite observations. Those exceptional locations of no significant fit may result from satellite track density at distinct areas. The results in the Polar Regions using

688 the SWAN-JRA-55 hindcast are not considered and discussed, considering that the ice
689 information was not considered during the wave hindcast simulation. Thus, the estimated
690 extreme waves resulting in areas of no significant fit to the GPD model should be carefully
691 considered.



692

693 **Figure 9.** Map showing the upper confidence intervals of the shape parameter (ξ) estimated
694 using the MLE method for SWAN-JRA-55 wave hindcast data (the first column), the
695 reanalysed ERA5 wave data (the second column), and satellite observation data (third column)
696 fitting a GPD. Each row corresponds to a distinct period.

697

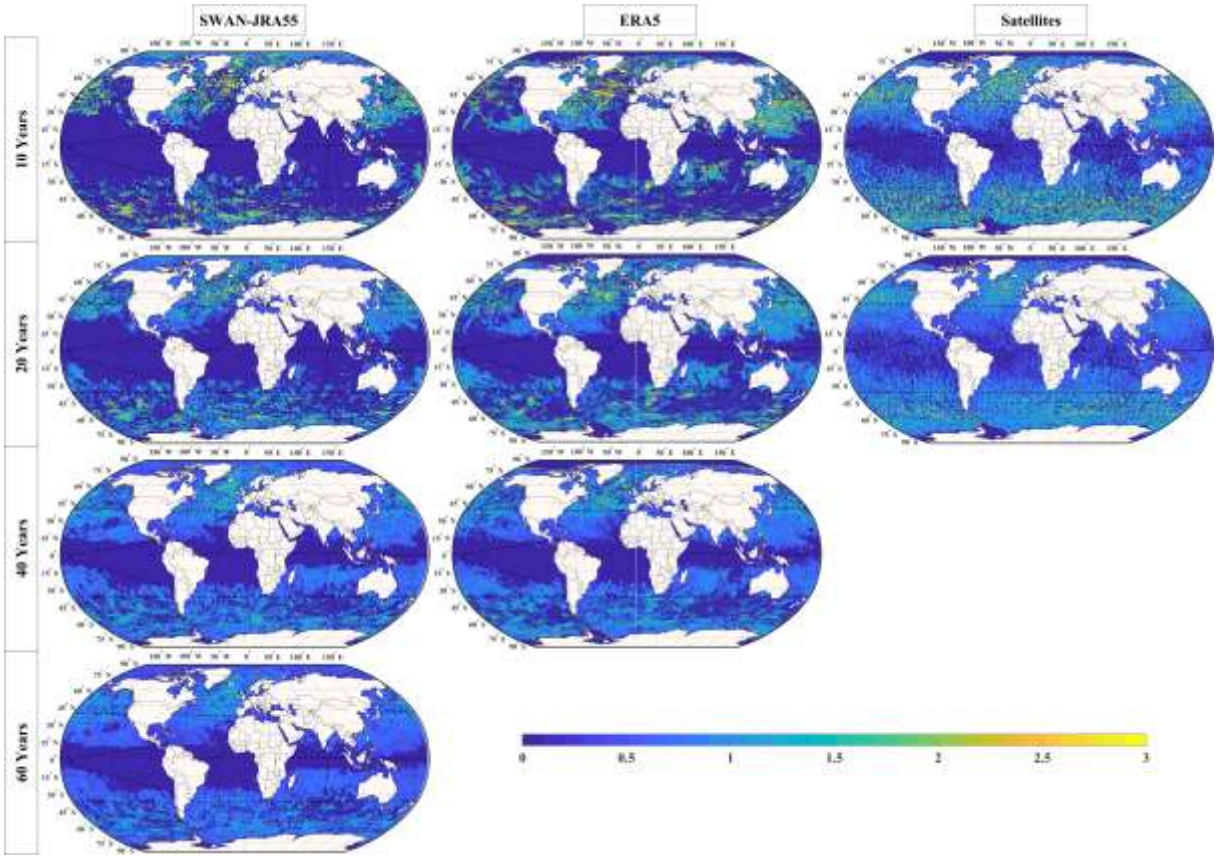


Figure 10. Map showing the upper confidence intervals of the scale parameter (σ) estimated using the MLE method for SWAN-JRA-55 wave hindcast data (the first column), the reanalysed ERA5 wave data (the second column), and satellite observation data (third column) fitting the GPD. Each row corresponds to a distinct period.

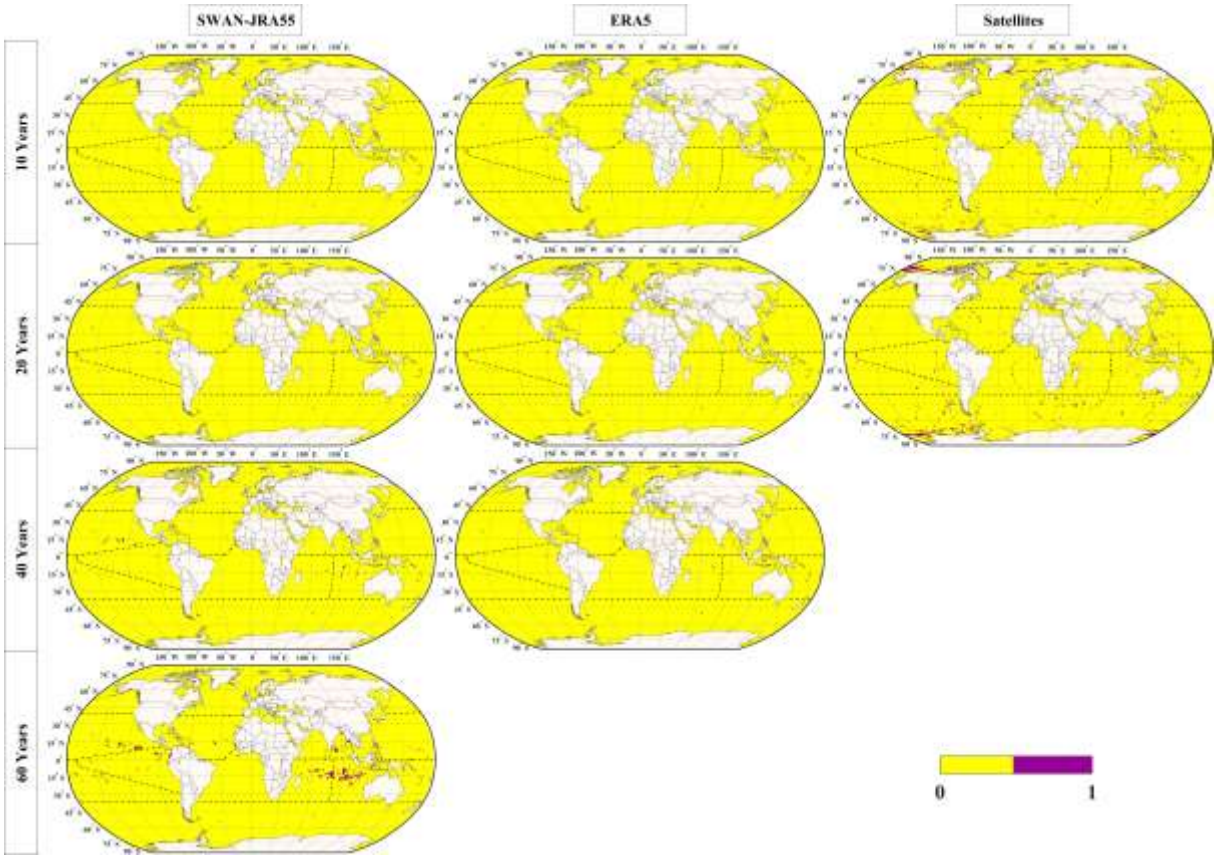


Figure 11. Map showing K-S test hypothesis results. In the yellow areas, the null hypothesis H_0 is maintained (The POT data fit GPD) at a risk level alpha=0.05, while in the purple areas, the null hypothesis H_0 is rejected. The results shown fit the SWH hindcast from SWAN-JRA-55 (the first column), the SWH data from ERA5 (the second column), and the satellite observation (the third column). Each row corresponds to a distinct sample size.

4.2.2. Extreme SWH estimates

The extreme SWHs discussed in this section are estimated using the POT-GPD model. Using the spatial datasets with different periods, the extreme SWHs with a 100-year return period are estimated (Figure 12) and compared (Figure 13). Over most of the globe, the extreme SWH results estimated from the ERA5 and SWAN-JRA-55 data showed a relative difference of <20% in large part of the world (Figure 13 (c)). The ERA5 results are higher compared to SWAN-JRA55 results in the north and south tropical regions and lower in the tropical areas. In the Polar Regions SWAN-JRA-55 extreme wave are overestimated compared to both satellite and ERA5 results. This over-estimation was expected as SWAN-JRA-55 simulations have been carried out without sea ice data. Comparing the results obtained based on satellite observations to those obtained based on ERA5 and SWAN-JRA55 (Figure 13 (a,b)), remarkable differences reaching 30% in a large part of the globe is noticed. The extreme values estimated

based on satellite data are lower in the North Atlantic, the North Pacific, the South Ocean, and in the polar regions. However, in the tropical region, the extreme values estimated based on satellite data are higher by 10% to 40%. The differences related to the data source used for the tropical zone are higher in the Arabian Sea.

The sensitivity of the estimated extreme values to the analysed period show also a dependence on the used data sources (Figure 13 (d-i)). The observed relative changes are more important using satellite observation and SWAN-JRA55. In large part of the world oceans, an increase of 10 to 20% in the estimated extreme SWH is observed by incising the analysed satellite data period from 10 years to 20 years (Figure 13 (f)). In the polar region, the relative differences are more important and can reach 40% with an increasing change in the Arctic and a decreasing change near the Antarctic.

Using SWAN-JRA55 datasets, the changes as a function of the considered period are more remarkable when shifting from 20 to 40 years (Figure 13 (g)) and less noticeable between 40 and 60 years (Figure 13 (i)). Using the POT-GPD model, a 40-year period may be considered sufficient for estimating the extreme SWH for a 100years return period in a large part of the world. However, the rate of change observed using 60 years (Figure 13 (i)) remains considérable in the Arabian sea, the north pacific, and the western Atlantic.

The lowest relative change as a function of the data period is computed by comparing the ERA5 results of 40, 20, and 10years periods (Figure 13 (e, h)). The relative changes are <10% in large parts of oceans and can reach 20% in several regions (Figure 13 (e, h)). In the north pole and the in the north Indian ocean, the estimated extreme SWH is decreasing by an increase in the analysed period of ERA5 data.

Compared to AM-GEV results, the POT-GPD results do not contain any outliers in the areas with high tropical cyclone activities. The extreme SWHs obtained using POT-GPD based on satellite observations are in line with those obtained by Takbash and Young (2019) and Takbash et al. (2019) in most of the globe. However, in the tropical west Pacific (Philippine sea), the results obtained by Takbash et al. (2019) are higher and reach 20 m, against 14 m in the present study. In this tropical cyclone zone, the results of the present study are more in line with those of Vinoth and Young (2011) obtained using the initial distribution method (IDM) approach.

Takbash and Young (2019) used a threshold fixed at the 90^{th} percentile, opposite to the selected threshold used in this study which depends on the wave data distribution at each location. Takbash and Young (2020) estimated the 100-year extreme SWH based on ERA5 data of 41

years using POT-GPD for a fixed threshold at the 70th percentile. The present satellite-based results are more similar to those obtained by Meucci et al. (2020), who used the POT approach with exponential distribution fit considering the threshold corresponding to the minimum highest 1000 peaks at each location.

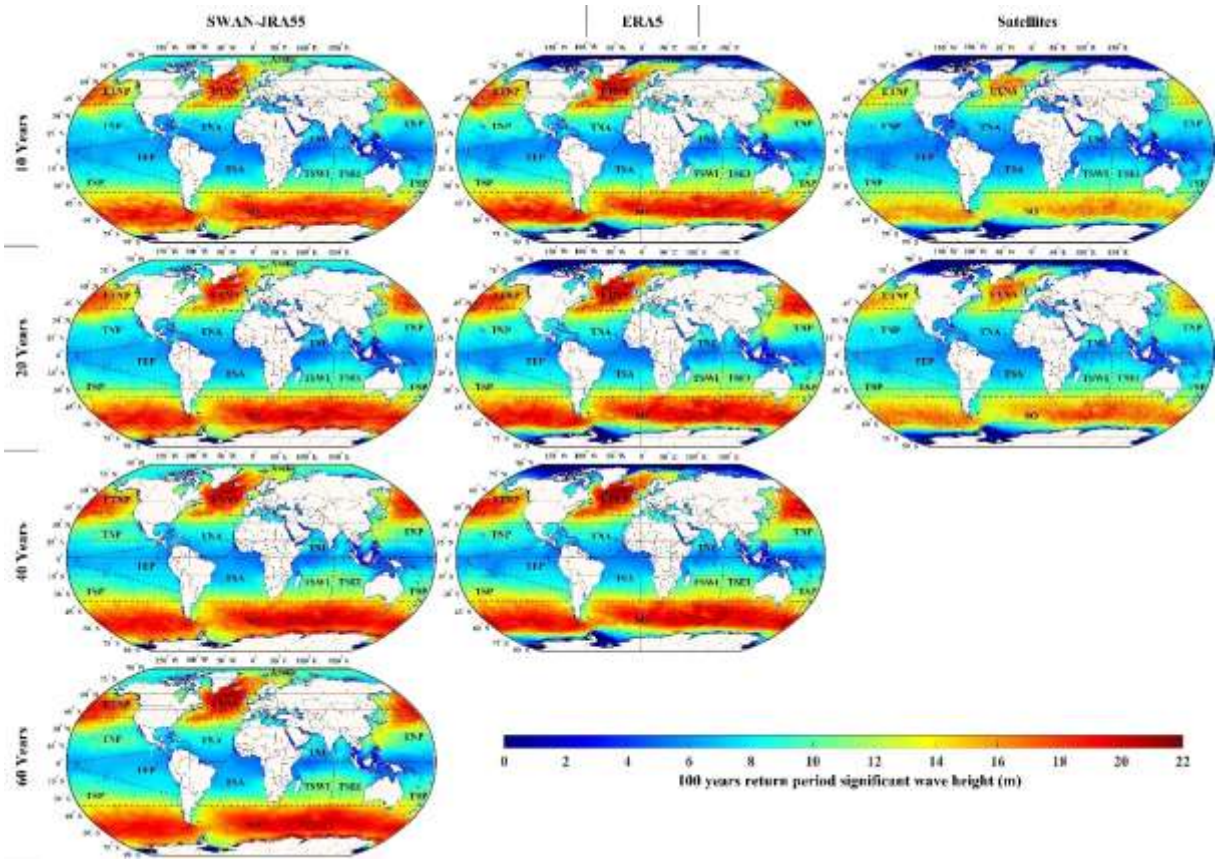


Figure 12. Extreme SWHs with 100-year return period estimated using POT-GPD model for SWAN-JRA-55 wave hindcast data (the first column), the ERA5 wave data (the second column), and satellite observation data (the third column). The maps in each row correspond to a distinct period.

Comparing the results obtained using a 40-year dataset of ERA5 (Figure 11) to those obtained by (Takbash and Young 2020), we noticed a suitable agreement in large part of the globe. However, the results show a significant difference in the semi-closed seas, such as the West Mediterranean Sea, the Black Sea, the Caspian Sea, the Arabian Sea, and the Gulf of Mexico. The results obtained at those locations may depend more on the selected threshold. According to (Takbash and Young 2019), the resulting extreme SWHs can vary by up to 30% depending on the threshold chosen. In another part, considerable differences in the estimated extreme SWHs at the Philippine Sea can be noticed. (Takbash and Young 2020) results show that the

extreme SWH in this location exceeds can 20 m. The differences in the obtained results at this location may also be related to the selected threshold.

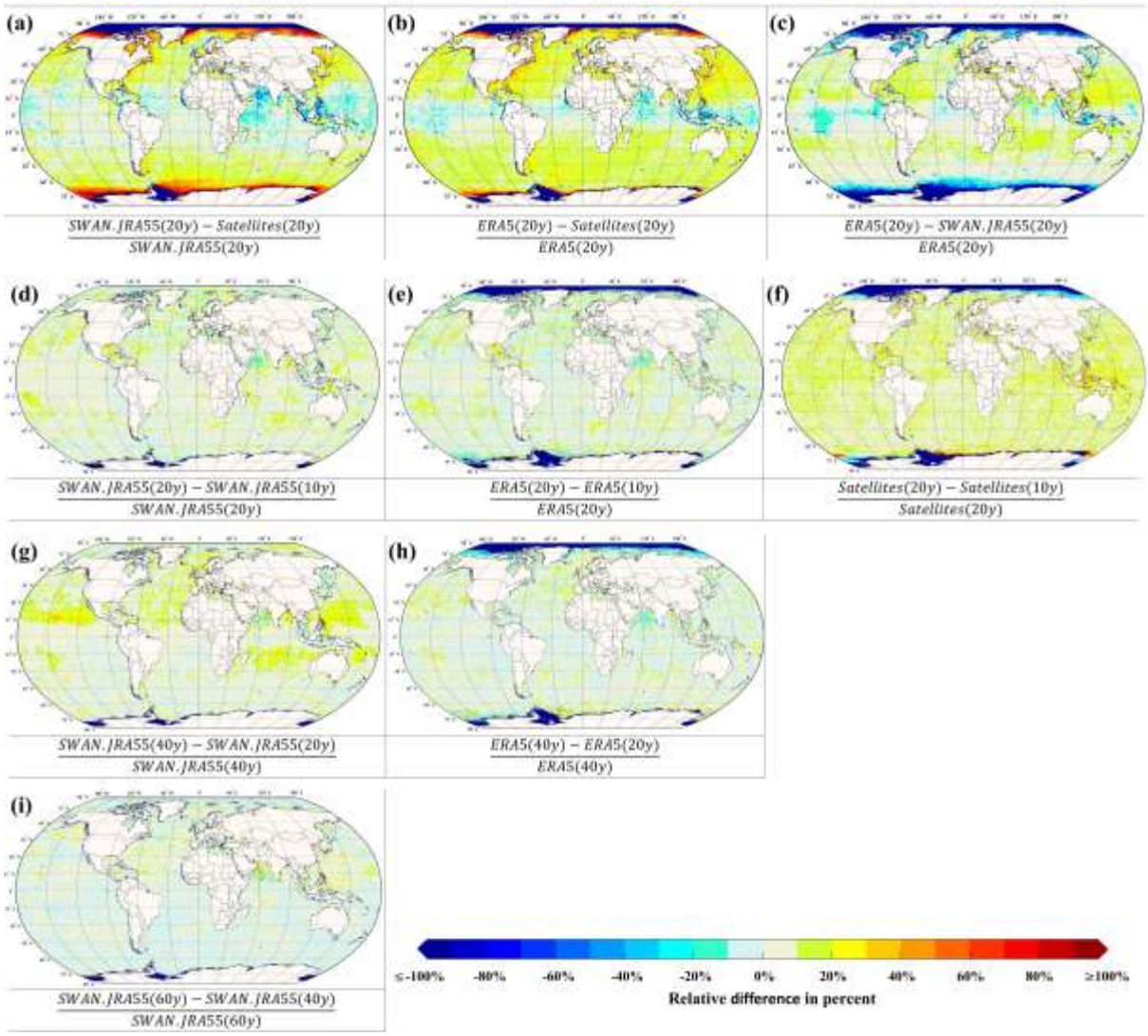


Figure 13. Maps showing the relative biases calculated by comparing the extreme significant wave height of the 100-year return period estimated using the POT-GPD based on different analysed data periods and data sources. The maps a-f show the biases when comparing the results obtained from various data periods within the same data source, and the maps h-j show the biases between the results obtained from three data sources for the same period of 20 years (20y).

4.2.3. Accuracy of the estimated extreme SWHs

Using the POT-GPD model, the extreme SWHs were estimated at six buoy locations for different return periods. The buoy-based results are compared to the ERA5-based and SWAN-JRA-55-based results (Figure 14). The ERA5 and SWAN-JRA-55 datasets match the buoy measurements in time and space. The threshold is estimated using the same approach presented in section 2.3, and the goodness of fit of each dataset exceeding the thresholds is tested based

on the K-S test. The selected threshold at all buoy locations and the K-S test results are shown in Table 3. Referring to the goodness of fit test (K-S test) results, we can notice that, even if the ERA5 and SWAN-JRA-55 data show a better fit of the GPD model with higher p-values, the estimated extreme SWHs are underestimated compared to all buoy measurements. Dentale et al. (2018) compare the extreme SWHs estimated using buoy measurements in the Gulf of Mexico (at B1, referring to the buoy 42002) and the ECMWF global wave model data. As a result, they show a considerable underestimation in extreme SWHs estimated based on the ECMWF. The results obtained using buoy measurement (B2) in Dentale et al. (2018) are similar to those obtained in the present study. Thus, the results obtained at B1 and B2 for a return period of 100 years are in line with those obtained at the same buoy locations by (Vinoth and Young 2011) and by (Alves and Young 2003).

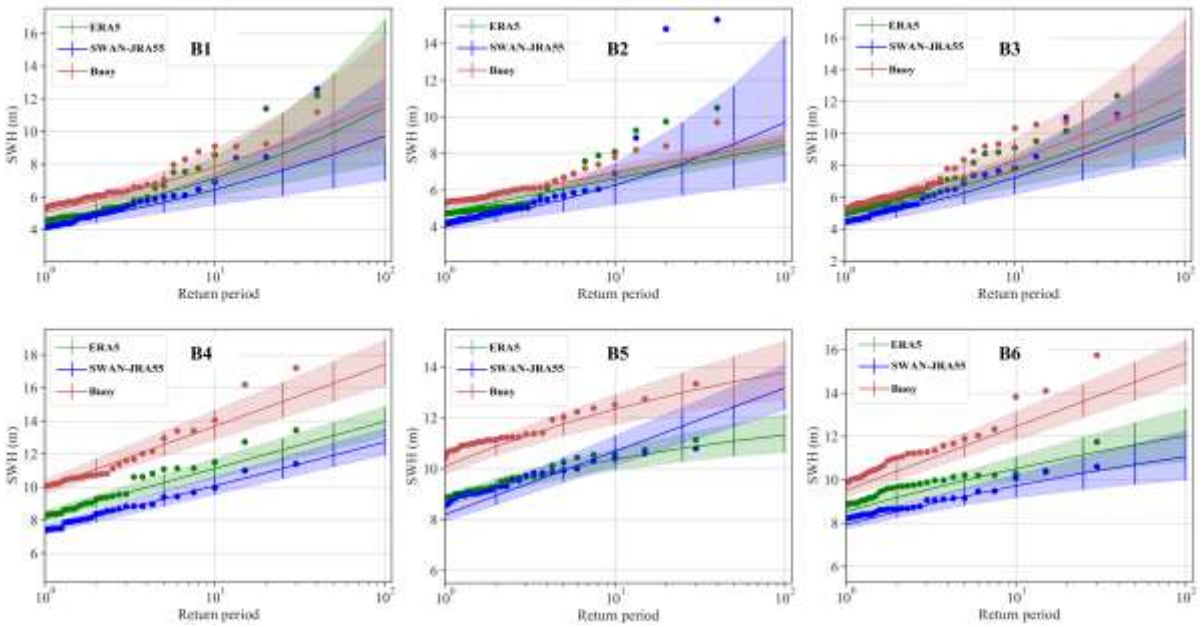


Figure 14. Extreme SWHs at different return periods estimated using on POT-GPD model at six buoy locations based on wave measurements, SWAN-JRA-55 wave hindcast, and ERA5 wave reanalyze. The shaded colour shows the confidence intervals for the risk of α=0.05.

Compared the POT-GPD results obtained based on buoy measurements to the AM-GEV results, we noticed that the extreme SWHs for a return period of 100 years are very close at all buoys except for B6, where the estimated values are higher using the AM-GEV model. As shown in the spatial results (Figures 8 and 14), the differences in the estimated extreme SWHs using AM-GEV and POT-GPD depend on the spatial location and the analysed data pe**3.** The selected

thresholds and p-values obtained as results of K-S test for buoy measurements exceeding thresholds and their corresponding ERA5 and SWAN-JRA-55 datasets. The null hypotheses are rejected if the p-value<0.05.

	SWH threshold (m)			K-S test p-value		
Locations	Buoys	ERA5	SWAN-JRA-55	Buoys	ERA5	SWAN-JRA-55
B1	3.40	3.15	2.63	0.343	0.516	0.688
B2	3.70	2.96	2.72	0.050	0.257	0.198
B3	2.96	2.69	2.17	0.339	0.743	0.709
B4	6.16	5.50	4.71	0.925	0.238	0.514
B5	6.93	6.48	5.90	0.997	0.886	0.596
B6	6.64	6.01	5.52	0.977	0.986	0.985

Using ERA5 and SWAN-JRA-55 datasets and the POT-GPD model, the estimated results are closer to buoy-based results compared to those obtained using AM-GEV model. Considering a larger sample of storm events using the POT approach can be more recommended to reduce the uncertainty related to the estimated maximum annual peaks. However, considering the limitation in buoy measurements worldwide and that the underestimations observed using ERA5 and SWAN-JRA-55 datasets may exceed 2 m, it is crucial to increase the buoy measurements around the world to avoid the risk related to an overestimation in an extreme SWH causing damage and economic losses in different coastal and offshore activities. As shown on the maps, extending the analysed period can increase or decrease the estimated extreme SWHs in large parts of the globe. It is therefore recommended to consider the reanalysis data period carefully as a function of the study area where no measurements are available. Thus, as ERA5-based results are closer to the measurements-based results, we strongly recommend using long-term ERA5 and the POT-GPD approach.

5. Conclusions

The study presents a global estimation of the extreme wave highs and investigates the sensitivity of the extreme wave estimates to the used data sources and the length of the analysed period. For this proposal, the extreme waves are estimated globally based on the wave hindcast data (SWAN-JRA-55) for 10, 20, 40, and 60 yearly periods, the reanalysed wave data (ERA5) of 10, 20, and 40 yearly periods, and the satellite altimetry observations of 10 and 20 yearly periods. Thus the extreme waves are estimated based on long-term measurements data of >30

years period obtained at six different locations and compared to the results obtained using reanalysed and hindcast data at the nearest grid points. The extreme value analysis was performed using two of the most used methods; the AM-GEV and the POT-GPD. The results were obtained both globally and at the buoy locations and allowed us to reach the following main conclusion:

- In most global regions, the AM and POT data of different periods and different sources show a significantly good fit to GEV and GPD distributions successively. However, the confidence interval of the estimated shape and scale parameters is high using 10 years of data and decreases by increasing the analysed data periods. Hence, the goodness of feet test may not be enough to evaluate the accuracy of the extreme wave model.
- The extreme wave estimates can change by >20% over most of the global ocean depending on the used wave sources, and therefore the choice of suitable sources must be carefully considered.
- The estimated extreme wave values increase as a function of the analysed data period from 10 years to 40 years. However, by increasing the period to 60 years, the results remain close to those observed using a 40 years period.
- Using the AM-GEV model, the results derived from both SWAN-JRA-55 and ERA5 waves, outliers in extreme wave values that reach 30 m, are estimated in tropical cyclone regions. The AM-GEV model is not recommended for tropical cyclone regions. Out of the tropical cyclone regions, relative differences are mainly <20% comparing the extreme SWH estimated based on SWAN-JRA-55 and ERA5 data to those estimated based on satellite observations.
- Using the POT-GPD model, the extreme wave values calculated using satellite observations are significantly lower than those computed using SWAN-JRA-55 and ERA5 datasets, except for the polar and equatorial regions. Satellites can avoid a range of peaks above the threshold with a revisit period of several days.
- Comparing the results obtained based on SWAN-JRA-55 and ERA5 datasets to those obtained using buoy measurements, we noticed an underestimation in the estimated extreme waves high, which reach 2 m in the North-East Pacific and in the North-West Atlantic, and an overestimation in the Gulf of Mexico, which is marked by considerable tropical cyclone activity. However, due to the lack of long-term buoy measurements in the global ocean, the use of hindcast data is indispensable. It is therefore recommended to improve global wind wave model accuracy in estimating the wave storm events peaks and tropical cyclone events.

- Although the SWAN-JRA5 and ERA5 historical waves are validated and show low biases and good correlation with wave measurements, their relative accuracy in estimating storm waves may not be sufficient for extreme wave analysis. Calibration or correction of historical data should be done in terms of storm waves and tropical cyclones.

Declarations

Ethical Approval

This declaration is “not applicable”

Competing interests

The authors have no conflicts of interest to declare that are relevant to the content of this article.

Authors' contributions

Khalid AMAROUCHE and Adem AKPINAR wrote the original draft. Bahareh KAMRANZAD and Khalid AMAROUCHE. performed the wave hindcast simulations. Khalid AMAROUCHE. wrote the main manuscript, collected and analyzed the data, validated the data. Khalid AMAROUCHE and Ghollame-Ellah-Yacine KHAMES performed the formal analysis and prepared the figures, Khalid AMAROUCHE., Adem AKPINAR and Bahareh KAMRANZAD reviewed the manuscript. Adem AKPINAR supervised the study.

Funding

The authors did not receive support from any organization for the submitted work.

Availability of data and material

The datasets generated during and/or analysed during the current study are available from the corresponding author on reasonable request.

Acknowledgments

We acknowledge the European Centre for Medium-Range Weather Forecasts (ECMWF) for providing wind data through the official website of the Copernicus Climate Change Service (C3S) Climate Data Store. We acknowledge as well Copernicus Marine Environment Monitoring Service (CMEMS) for providing wave measurements. Also, the authors recognize the Institut Français de Recherche pour l'Exploitation de la Mer (Ifremer) for providing the corrected satellites observations and the General Bathymetric Chart of the Oceans (GEBCO) for delivering the bathymetry data.

References

Aarnes O, Breivik Ø, Climate MR-J of, 2012 undefined Wave extremes in the northeast Atlantic. journals.ametsoc.org

Abdalla S, Dinardo S, Benveniste J, Janssen PAEM (2018) Assessment of CryoSat-2 SAR mode wind and wave data. Adv Sp Res 62:1421–1433. https://doi.org/10.1016/j.asr.2018.01.044

Agarwal A, Venugopal V, Harrison GP (2013) The assessment of extreme wave analysis methods applied to potential marine energy sites using numerical model data. Renew Sustain Energy Rev 27:244–257. https://doi.org/10.1016/J.RSER.2013.06.049

Alves JHGM, Young IR (2003) On estimating extreme wave heights using combined Geosat, Topex/Poseidon and ERS-1 altimeter data. Appl Ocean Res 25:167–186. https://doi.org/10.1016/J.APOR.2004.01.002

Amarouche K, Akpınar A, Semedo A (2021a) Wave storm events in the Western Mediterranean Sea over four decades. Ocean Model 170:101933. https://doi.org/10.1016/J.OCEMOD.2021.101933

Amarouche K, Akpınar A, Soran MB, et al (2021b) Spatial calibration of an unstructured SWAN model forced with CFSR and ERA5 winds for the Black and Azov Seas. Appl Ocean Res 117:102962. https://doi.org/10.1016/J.APOR.2021.102962

Bernardara P, Mazas F, Kergadallan X, Hamm L (2014) A two-step framework for over-threshold modelling of environmental extremes. Nat Hazards Earth Syst Sci 14:635–647. https://doi.org/10.5194/NHESS-14-635-2014

931 Booij N, Ris RC, Holthuijsen LH (1999) A third-generation wave model for coastal
932 regions: 1. Model description and validation. J Geophys Res 104:7649–7666.
933 https://doi.org/10.1029/98JC02622

934 Butturi-Gomes D, Beijo LA, Avelar FG (2019) On modeling the maximum duration
935 of dry spells: a simulation study under a Bayesian approach. Theor Appl Climatol
936 137:1337–1346. https://doi.org/10.1007/S00704-018-2684-1/FIGURES/5

937 Buxton I, Stephenson G (2001) Evaluating Design For UpgradeabilityA Simulation
938 Based Approach For Ships and Marine Products

939 Cai Y, Hames D (2010) Minimum sample size determination for generalized extreme
940 value distribution. Commun Stat - Simul Comput 40:87–98.
941 https://doi.org/10.1080/03610918.2010.530368

942 Caires S (2016) A Comparative Simulation Study of the Annual Maxima and the
943 Peaks-Over-Threshold Methods. J Offshore Mech Arct Eng 138:.
944 https://doi.org/10.1115/1.4033563

945 Caires S, Swail VR, Wang XL (2006) Projection and Analysis of Extreme Wave
946 Climate. J Clim 19:5581–5605. https://doi.org/10.1175/JCLI3918.1

947 Campos RM, Guedes Soares C, Alves JHGM, et al (2019) Regional long-term
948 extreme wave analysis using hindcast data from the South Atlantic Ocean. Ocean Eng
949 179:202–212. https://doi.org/10.1016/J.OCEANENG.2019.03.023

950 Cañellas B, Orfila A, Mendez FJ, et al (2007) Application of a POT model to estimate
951 the extreme significant wave height levels around the Balearic Sea (Western
952 Mediterranean)

953 Chandra M, Singpurwalla ND, Stephens MA (1981) Kolmogorov Statistics for Tests
954 of Fit for the Extreme Value and Weibull Distributions. J Am Stat Assoc 76:729.
955 https://doi.org/10.2307/2287539

956 Coles S (2001) An Introduction to Statistical Modeling of Extreme Values. pp 1–17

957 De Alfonso M, Manzano F, Gallardo A (2022) Quality information document For
958 REProcessed IN SITU product: Insitu_Glo_Wav_Rep_Observation_013_045

959 Dee DP, Uppala SM, Simmons AJ, et al (2011) The ERA-Interim reanalysis:
960 configuration and performance of the data assimilation system. Q J R Meteorol Soc

137:553–597. https://doi.org/10.1002/qj.828

Dentale F, Furcolo P, Carratelli EP, et al (2018) Extreme Wave Analysis by Integrating Model and Wave Buoy Data. Water 2018, Vol 10, Page 373 10:373. https://doi.org/10.3390/W10040373

Durrant TH, Greenslade DJM, Simmonds I (2009) Validation of Jason-1 and Envisat Remotely Sensed Wave Heights. J Atmos Ocean Technol 26:123–134. https://doi.org/10.1175/2008JTECHO598.1

Elgohari H, Yousof HM (2021) A New Extreme Value Model with Different Copula, Statistical Properties and Applications. Pakistan J Stat Oper Res 17:1015–1035. https://doi.org/10.18187/pjsor.v17i4.3471

Fisher RA (1925) Theory of Statistical Estimation. Math Proc Cambridge Philos Soc 22:700–725. https://doi.org/10.1017/S0305004100009580

Goda Y (2000) Random Seas and Design of Maritime Structures. WORLD SCIENTIFIC

Goda Y (2010) Random Seas and Design of Maritime Structures. WORLD SCIENTIFIC

Grabemann I, Weisse R, Grabemann I, Weisse R (2008) Climate change impact on extreme wave conditions in the North Sea: an ensemble study. OcDyn 58:199–212. https://doi.org/10.1007/S10236-008-0141-X

Gramcianinov CB, Campos RM, Guedes Soares C, Camargo R de (2020) Extreme waves generated by cyclonic winds in the western portion of the South Atlantic Ocean. Ocean Eng 213:107745. https://doi.org/10.1016/J.OCEANENG.2020.107745

Hasselmann K, Barnett TP, Bouws E, et al (1973) Measurements of wind−wave growth and swell decay during the Joint North Sea Wave Project (JONSWAP). Ergänzung zur Deut Hydrogr Z 12:1–95

Hasselmann S, Hasselmann K, Allender JH, Barnett TP (1985) Computations and Parameterizations of the Nonlinear Energy Transfer in a Gravity-Wave Specturm. Part II: Parameterizations of the Nonlinear Energy Transfer for Application in Wave Models. J Phys Oceanogr 15:1378–1391. https://doi.org/10.1175/1520-0485(1985)015<1378:CAPOTN>2.0.CO;2

Hersbach H, Bell B, Berrisford P, et al (2020) The ERA5 global reanalysis. Q J R Meteorol Soc 146:1999–2049. https://doi.org/10.1002/qj.3803

Hithin NK, Remya PG, Balakrishnan Nair TM, et al (2015) Validation and Intercomparison of SARAL/AltiKa and PISTACH-Derived Coastal Wave Heights Using In-Situ Measurements. IEEE J Sel Top Appl Earth Obs Remote Sens 8:4120–4129. https://doi.org/10.1109/JSTARS.2015.2418251

Jeong C, Panchang VG (2008) Measurement-based estimates of extreme wave conditions for the Gulf of Mexico. Ocean 2008. https://doi.org/10.1109/OCEANS.2008.5151997

Kamranzad B, Amarouche K, Akpinar A (2022) Linking the long-term variability in global wave energy to swell climate and redefining suitable coasts for energy exploitation. Sci Reports 2022 121 12:1–16. https://doi.org/10.1038/s41598-022-18935-w

Kamranzad B, Lavidas G, Takara K (2020) Spatio-Temporal Assessment of Climate Change Impact on Wave Energy Resources Using Various Time Dependent Criteria. Energies 13:768. https://doi.org/https://doi.org/10.3390/en13030768

Kamranzad B, Mori N (2019) Future wind and wave climate projections in the Indian Ocean based on a super-high-resolution MRI-AGCM3.2S model projection. Clim Dyn 53:. https://doi.org/10.1007/s00382-019-04861-7

Kendall M, Alan S (1961) The advanced theory of statistics

Komen GJ, Hasselmann K, Hasselmann K (1984) On the Existence of a Fully Developed Wind-Sea Spectrum. J Phys Oceanogr 14:1271–1285. https://doi.org/10.1175/1520-0485(1984)014<1271:OTEOAF>2.0.CO;2

Leben RR, Powell BS (2010) Accuracy Assessment of Jason-1 and TOPEX/POSEIDON Along-Track Sea Surface Slope Special Issue: Jason-1 Calibration/Validation. http://dx.doi.org/101080/714044526 26:355–366. https://doi.org/10.1080/714044526

Lee-Lueng Fu (1994) TOPEX/POSEIDON mission overview. J Geophys Res 99:. https://doi.org/10.1029/94JC01761

Liang B, Gao H, Shao Z (2019) Characteristics of global waves based on the third-

generation wave model SWAN. Mar Struct 64:35–55. https://doi.org/10.1016/j.marstruc.2018.10.011

Lobeto H, Menendez M, Losada IJ (2021) Future behavior of wind wave extremes due to climate change. Sci Rep 11:7869. https://doi.org/10.1038/s41598-021-86524-4

Martins ALA, Liska GR, Beijo LA, et al (2020) Generalized Pareto distribution applied to the analysis of maximum rainfall events in Uruguaiana, RS, Brazil. SN Appl Sci 2:1–13. https://doi.org/10.1007/S42452-020-03199-8/TABLES/5

Mathiesen M, Goda Y, Hawkes PJ, et al (1994) Recommended practice for extreme wave analysis. J Hydraul Res 32:803–814. https://doi.org/10.1080/00221689409498691

Mazas F, Hamm L (2011) A multi-distribution approach to POT methods for determining extreme wave heights. Coast Eng 58:385–394. https://doi.org/10.1016/J.COASTALENG.2010.12.003

Meucci A, Young IR, Aarnes OJ, Breivik Ø (2020) Comparison of wind speed and wave height trends from twentieth-century models and satellite altimeters. J Clim 33:611–624. https://doi.org/10.1175/JCLI-D-19-0540.1

Mínguez R, Tomás A, Méndez FJ, Medina R (2013) Mixed extreme wave climate model for reanalysis databases. Stoch Environ Res Risk Assess 27:757–768. https://doi.org/10.1007/S00477-012-0604-Y/FIGURES/7

Mori N, Yasuda T, Mase H, et al (2010) Projection of Extreme Wave Climate Change under Global Warming. Hydrol Res Lett 4:15–19. https://doi.org/10.3178/hrl.4.15

Murakami H (2014) Tropical cyclones in reanalysis data sets. Geophys Res Lett 41:2133–2141. https://doi.org/10.1002/2014GL059519

Neary VS, Ahn S, Seng BE, et al (2020) Characterization of Extreme Wave Conditions for Wave Energy Converter Design and Project Risk Assessment. J Mar Sci Eng 2020, Vol 8, Page 289 8:289. https://doi.org/10.3390/JMSE8040289

Nicolae Lerma A, Bulteau T, Lecacheux S, Idier D (2015) Spatial variability of extreme wave height along the Atlantic and channel French coast. Ocean Eng 97:175–185. https://doi.org/10.1016/J.OCEANENG.2015.01.015

O'Grady JG, Stephenson AG, McInnes KL (2022) Gauging mixed climate extreme value distributions in tropical cyclone regions. Sci Reports 2022 121 12:1–9.

https://doi.org/10.1038/s41598-022-08382-y

Orimolade AP, Haver S, Gudmestad OT (2016) Estimation of extreme significant wave heights and the associated uncertainties: A case study using NORA10 hindcast data for the Barents Sea. Mar Struct 49:1–17. https://doi.org/10.1016/J.MARSTRUC.2016.05.004

Panchang V, Jeong CK, Demirbilek Z (2013) Analyses of extreme wave heights in the gulf of mexico for offshore engineering applications. J Offshore Mech Arct Eng 135:1–15. https://doi.org/10.1115/1.4023205/376962

Queffeulou P (2010) Long-Term Validation of Wave Height Measurements from Altimeters. Geod Mar 27:495–510. https://doi.org/10.1080/01490410490883478

Queffeulou P, Croize-Fillonr D (2017) Global altimeter SWH data set–February 2017. Plouzané, France

Ris RC, Holthuijsen LH, Booij N (1999) A third-generation wave model for coastal regions: 2. Verification. J Geophys Res 104:7667–7681. https://doi.org/10.1029/1998JC900123

Saeed Far S, Abd. Wahab AK (2016) Evaluation of Peaks-Over-Threshold Method. Ocean Sci Discuss 1–25. https://doi.org/10.5194/os-2016-47

Samayam S, Laface V, Annamalaisamy SS, et al (2017) Assessment of reliability of extreme wave height prediction models. Nat Hazards Earth Syst Sci 17:409–421. https://doi.org/10.5194/nhess-17-409-2017

Sartini L, Cassola F, Besio G (2015a) Extreme waves seasonality analysis: An application in the Mediterranean Sea. J Geophys Res Ocean 120:6266–6288. https://doi.org/10.1002/2015JC011061

Sartini L, Mentaschi L, Besio G (2015b) Comparing different extreme wave analysis models for wave climate assessment along the Italian coast. undefined 100:37–47. https://doi.org/10.1016/J.COASTALENG.2015.03.006

Soran MB, Amarouche K, Akpınar A (2022) Spatial calibration of WAVEWATCH III model against satellite observations using different input and dissipation parameterizations in the Black Sea. Ocean Eng 257:111627. https://doi.org/10.1016/J.OCEANENG.2022.111627

Soukissian TH, Kalantzi GD (2006) Extreme Value Analysis Methods Used For Extreme Wave Prediction

Soukissian TH, Tsalis C (2015) The effect of the generalized extreme value distribution parameter estimation methods in extreme wind speed prediction. Nat Hazards 78:1777–1809. https://doi.org/10.1007/S11069-015-1800-0/TABLES/4

Sulis A, Cozza R, Annis A (2017) Extreme wave analysis methods in the gulf of Cagliari (South Sardinia, Italy). Ocean Coast Manag 140:79–87. https://doi.org/10.1016/J.OCECOAMAN.2017.02.023

Takbash A, Young IR (2020) Long-Term and Seasonal Trends in Global Wave Height Extremes Derived from ERA-5 Reanalysis Data. J Mar Sci Eng 2020, Vol 8, Page 1015 8:1015. https://doi.org/10.3390/JMSE8121015

Takbash A, Young IR (2019) Global Ocean Extreme Wave Heights from Spatial Ensemble Data. J Clim 32:6823–6836. https://doi.org/10.1175/JCLI-D-19-0255.1

Takbash A, Young IR, Breivik Ø (2019) Global Wind Speed and Wave Height Extremes Derived from Long-Duration Satellite Records. J Clim 32:109–126. https://doi.org/10.1175/JCLI-D-18-0520.1

Thomas M, Lemaitre M, Wilson ML, et al (2016) Applications of Extreme Value Theory in Public Health. PLoS One 11:e0159312. https://doi.org/10.1371/JOURNAL.PONE.0159312

Van Vledder GP, Goda Y, Hawkes P, et al (1994) Case Studies of Extreme Wave Analysis: A Comparative Analysis. In: Proceedings Waves 93', Ocean Wave Measurement and Analysis. American Society of Civil Engineers (ASCE), pp 978–992

Vecchi GA, Delworth T, Gudgel R, et al (2014) On the Seasonal Forecasting of Regional Tropical Cyclone Activity. J Clim 27:7994–8016. https://doi.org/10.1175/JCLI-D-14-00158.1

Vieira BFV, Pinho JLS, Barros JAO (2021) Extreme wave value analysis under uncertainty of climate change scenarios off Iberian Peninsula coast. Ocean Eng 229:109018. https://doi.org/10.1016/J.OCEANENG.2021.109018

Vinoth J, Young IR (2011) Global Estimates of Extreme Wind Speed and Wave Height. J Clim 24:1647–1665. https://doi.org/10.1175/2010JCLI3680.1

Wada R, Waseda T (2020) Assessment of Data-Inherited Uncertainty in Extreme Wave Analysis. J Offshore Mech Arct Eng 142:. https://doi.org/10.1115/1.4045621/1071465

Wada R, Waseda T (2018) Benchmark for the Sources of Uncertainty in Extreme Wave Analysis. Proc Int Conf Offshore Mech Arct Eng - OMAE 3:. https://doi.org/10.1115/OMAE2018-78216

Wilks DS (2011) Statistical Methods in the Atmospheric Sciences. Stat Methods Atmos Sci 100:100

Wilks SS (1938) The Large-Sample Distribution of the Likelihood Ratio for Testing Composite Hypotheses on JSTOR. Ann Math Stat 9:60–62

Yang S, Oh J (2018) Long-Term Changes in the Extreme Significant Wave Heights on the Western North Pacific: Impacts of Tropical Cyclone Activity and ENSO. Asia-Pacific J Atmos Sci 54:103–109. https://doi.org/10.1007/s13143-017-0063-y

Yang Z, Neary VS, Wang T, et al (2017) A wave model test bed study for wave energy resource characterization. Renew Energy 114:132–144. https://doi.org/10.1016/j.renene.2016.12.057

Young IR, Vinoth J, Zieger S, Babanin A V. (2012) Investigation of trends in extreme value wave height and wind speed. J Geophys Res Ocean 117:0–06. https://doi.org/10.1029/2011JC007753

Yuan J, Emura K, Farnham C, Alam MA (2018) Frequency analysis of annual maximum hourly precipitation and determination of best fit probability distribution for regions in Japan. Urban Clim 24:276–286. https://doi.org/10.1016/J.UCLIM.2017.07.008

Zar JH (2013) Biostatistical analysis, 5th edn. Pearson